THE JOURNAL OF PHYSICAL CHEMISTRY A

A: Spectroscopy, Molecular Structure, and Quantum Chemistry

Conformational Landscape and Polymorphism in 5-Acetic Acid Hydantoin

Bernardo Albuquerque N, Gulce Ogruc Ildiz, João Canotilho, M. Ermelinda S. Eusébio, Marta Sofia C. Henriques, José A. Paixão, and Rui Fausto

J. Phys. Chem. A, **Just Accepted Manuscript** • DOI: 10.1021/acs.jpca.0c03789 • Publication Date (Web): 08 Jun 2020

Conformational Landscape and Polymorphism in 5-Acetic Acid Hydantoin

B. A. Nogueira,[1,*] G. O. Ildiz,[1,2,*] J. Canotilho,[3] M. E. S. Eusébio,[1]
M. S. C. Henriques,[4] J. A. Paixão[4] and R. Fausto[1]

[1] *University of Coimbra, CQC, Department of Chemistry, P-3004-535 Coimbra, Portugal.*
[2] *Faculty of Sciences and Letters, Department of Physics, Istanbul Kultur University, Atakoy Campus, Bakirkoy 34156, Istanbul, Turkey.*
[3] *University of Coimbra, Faculty of Pharmacy, Coimbra, Portugal.*
[4] *University of Coimbra, CFisUC, Department of Physics, P-3004-516 Coimbra, Portugal.*

Abstract

The conformational space of 5-acetic acid hydantoin {5AAH; [2-(2,5-dioxoimidazolidin-4-yl)acetic acid]} was investigated by quantum chemical calculations performed at the DFT(B3LYP)/6-311++G(d,p) level of theory. A total of 13 conformers were located in the potential energy surface of the molecule, 6 of them bearing the carboxylic group in the *cis* arrangement (O=C–O–H dihedral equal to ~0º) and the other 7 possessing this group in the *trans* configuration (O=C–O–H dihedral equal to ~180º). The most stable conformer (*cis*-**I**) was trapped from the gas phase into a low temperature argon matrix (10 K), and its infrared spectrum was fully assigned, also with help of results of normal coordinates' analysis based on the DFT computed vibrational data. The electronic structure of this conformer was analyzed by using the Natural Bond Orbital (NBO) method.

The investigation of the thermal properties of 5-AAH was undertaken by differential scanning calorimetry (DSC), polarized light thermal microscopy (PLTM) and Raman spectroscopy, allowing identification of five different polymorphs. Very interestingly, in the room temperature stable polymorph the molecular units of 5-AAH assume the geometry of the highest-energy conformer predicted by the calculations for the isolated molecule.

* Corresponding authors' e-mails: ban@qui.uc.pt; g.ogruc@iku.edu.tr

1. Introduction

We have recently started a research program on the study of derivatives of hydantoin, focusing on their structure and electron distribution characteristics, vibrational spectra, photochemistry and thermal properties.[1-4] The parent hydantoin and its 1-methyl and 5-methyl derivatives were the first targeted compounds, mostly due to their intrinsic structural simplicity, including the fact that they can exist only in a single stable conformation.

Those previous studies[1-4] allowed us to establish the basic properties of the hydantoin moiety. For example, the structural analysis showed that the studied hydantoins have a planar (for hydantoin and 1-methyl hydantoin[1-3]) or quasi/planar (5-methyl hydantoin[4]) ring, sharing common geometrical and electronic features: to mention just some of the most important ones, (i) the relative lengths of the two distinct C=O bonds in the ring are dictated by the degree of π electronic delocalization from the nitrogen atoms, being longer when the C=O fragment is connected to two nitrogen atoms than when connected to a single nitrogen; (ii) the internal angles of the ring with a nitrogen atom in the apex are much larger (around 113º) than those with carbon atoms in the apex (~101-106º), due to different *s vs. p* compositions of the hybrid orbitals of the N and C atoms used to make the ring bonds; (iii) the π charge of the oxygen atom of the carbonyl group connected to two nitrogen atoms is more negative than that of the oxygen atom of the second carbonyl group (connected to a single nitrogen atom), in agreement with its longer bond length and involvement in a more extended π delocalization; and (iv) the σ charges of the two oxygen atoms are considerably less negative than the corresponding π charges and have opposite relative values, showing that a larger π bond polarization towards the oxygen atom leads to reduce the trend for the associated σ bond to be polarized in the same direction. These structural characteristics have relevant consequences for the reactivity of the hydantoin moiety, as demonstrated in the case of the previously reported photochemical preferred reaction channels exhibited by this type of molecules.[2-4]

Hydantoins are also prone to display polymorphism,[3-5] though only one crystalline structure has been reported for the parent compound hitherto.[6] For 1-methyl hydantoin, two different polymorphs have been described,[3] while 5-methyl hydantoin exhibits at least four

polymorphs, which were found to be stable enough at room temperature to be characterized experimentally.[4] Both asymmetry in the molecular unit and conformational flexibility are potentially relevant factors to increase the trend for a given compound to exist in different crystalline varieties, the first being possibly in the origin of the greater ability of the asymmetrically substituted (chiral) 5-methyl substituted hydantoin to render a larger number of different polymorphs, compared to the symmetric (non-chiral) 1-methyl derivative.

In the present study, we focus on 5-acetic acid hydantoin {5AAH; [2-(2,5-dioxoimidazolidin-4-yl)acetic acid]}, which is an asymmetrically substituted hydantoin bearing a conformationally flexible substituent group (Scheme 1).

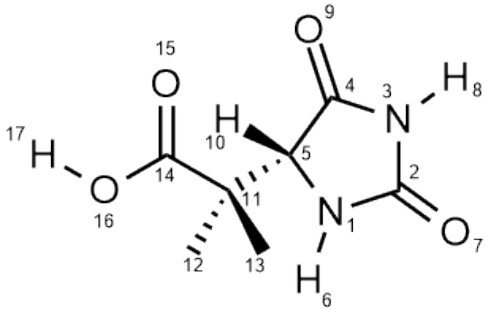

Scheme 1. The 5-acetic acid hydantoin molecule with the adopted atom numbering.

The justification for our interest in hydantoins result from the fact that they have been shown to be important in several domains, in particular in pharmacy and medicine. Since the introduction in the market of phenythoin (5,5-diphenyl hydantoin), first as anticonvulsant (as early as in 1938)[7] and later on as a medicine for myotonic muscular dystrophy treatment[8] and trigeminal neuralgia,[9] several other hydantoin-based drugs were discovered that have been clinically used as antiepileptic and antibacterial drugs,[10,11] and for cancer and AIDS treatments.[12-15] Hydantoins have been receiving also applications in agriculture as fungicides and herbicides.[16,17] Recently, some hydantoin derivatives based systems were also described as stimuli-responsive materials.[18]

Asymmetrically substituted hydantoins at position-5 are particularly interesting from the structural point of view because they are chiral. 5-Acetic acid hydantoin has been reported to possess antitumor activity, being effective against both asparaginase-sensitive and -resistant 6C3HED tumors (lymphoma).[19] It is a product resulting from elimination from the body of histamine, [20,21] which is known to strongly increase its concentration in the blood upon vitamin C depletion.[22] 5AAH is also currently used in synthesis of anti-inflammatory and analgesic active

compounds.[23] In addition, it has been shown to be a resourceful ligand in coordination chemistry.[24,25] In fact, besides the general attributes of the hydantoin ligand (more than one donor and acceptor atoms; ability to act either as neutral or deprotonated monoanionic species), 5AAH exhibits also characteristic features due to its carboxylic group substituent, which expand its coordination versatility, and makes this compound a good starting material for making metallo-organic frameworks, porous materials, and supra-molecular structures.[25]

In spite of its practical relevance,[19-25] investigation on the *a priori* interesting structural characteristics of 5AAH is practically inexistent. On the other hand, such knowledge can certainly facilitate the understanding of the role of 5AAH in the biochemical processes in which it participates, and may also provide relevant indications for its use in other areas, like synthetic and coordination chemistry. The present study then aimed to provide fundamental information on the compound, starting from a detailed characterization of its conformational space and molecular structure, going through the investigation of the vibrational (infrared) spectrum of the isolated molecule, till the search for different crystalline polymorphs of the neat compound and their structural, thermal and spectroscopic characterization. To achieve these goals, matrix isolation infrared spectroscopy was used, together with Density Functional Theory (DFT) calculations, for investigation of the singe molecule of the compound, while a combined approach by X-ray diffraction (XRD), differential scanning calorimetry (DSC), polarized light thermomicroscopy (PLTM), and Raman spectroscopy was applied to the study of the neat condensed phases. As it will be shown in details below, 5AAH exhibits several polymorphs. Remarkably, in the room temperature most stable polymorph, whose structure has been refined in the present study, the conformer selected to make the crystal corresponds to the highest-energy form of the isolated molecule.

2. Experimental and computational methods

5-Acetic acid hydantoin (98% purity; racemic) was obtained from Sigma-Aldrich and used without further purification. The cryogenic matrices were prepared by sublimation of 5AAH from a mini-furnace placed inside the cryostat (APD Cryogenics closed-cycle helium refrigeration system, with a DE-202A expander), and co-deposition of the generated vapors of the compound with argon (Air Liquide, N60) onto a CsI window mounted at the cold (10 K) tip of the cryostat. The temperature of the sample was controlled (Scientific Instruments, model 9650-1) by a silicon diode sensor, with an accuracy of 0.1 degrees.

Infrared spectra of the matrix-isolated compound were recorded using a Nicolet 6700 Fourier Transform infrared spectrometer with 0.5 cm^{-1} resolution. Raman spectra of the polymorphs were obtained using a Horiba LabRam HR Evolution micro-Raman system, with excitation at 632.8 nm (He-Ne laser), spectral resolution 1.5 cm^{-1}, 100x magnification objective (spot size 0.85 μm), acquisition time of 60 s, 10 accumulations, and laser power ~17 mW. In the spectral region of interest, the frequency accuracy is better than 0.5 cm^{-1}.

DSC analyses were done using a Perkin-Elmer Pyris-1 power compensation calorimeter, with a 1:1 v/v ethylene glycol-water cooler at –25º C and a 20 mL min^{-1} nitrogen purge flow. Aluminum pans (hermetically sealed) were used (samples weight between 1.2 and 2.0 mg), with an empty pan used as reference. Indium (Perkin-Elmer, 99.99%, T_{fus} = 156.60 ºC) and biphenyl (CRM LGC, T_{fus} = 68.93ºC ± 0.03 ºC)[26] were used for temperature and enthalpy calibrations. In the experiments, the samples were scanned from 25 to 222 ºC at a scan rate of 10 ºC min^{-1}. Polarized light thermal microscopy (PLTM) was used to collect images (200x) of the compound within the range of temperature of the DSC experiments. The used system includes a DSC600 Linkam hot stage attached to a Leica DMRB microscope and to a Sony CCD-IRIS/RGB video camera. The analysis of the images was done with the Linkam Real Time Video Measurement System software.

Recrystallization from different solvents were used for polymorph screening. In these experiments 5AAH (*ca.* 35 mg) solutions in dichloromethane, 1,4-dioxane, tetrahydrofuran (THF), acetone, water, methanol and ethanol (with volumes of 4 to 20 mL) were prepared and allowed to evaporate at room temperature. The polymorphs were characterized by micro-Raman spectroscopy.

Single crystal X-ray diffraction data for the stable room temperature polymorph of the compound (which is the product obtained by recrystallization from dichloromethane, acetone, water, methanol and ethanol) were collected on a Bruker APEXII diffractometer (Mo Kα radiation, graphite monochromator, λ = 0.71073 Å) using φ and ω scans. Data integration and scaling were performed with the SAINT suite of programs[27] and SADABS[27] was used for empirical absorption collection based on the measurement of a large set of redundant reflections. The structure was solved by direct methods using SHELXT-2014/5,[28] and full-matrix least squares refinement of the structural model was performed by SHELXL-2018/2.[29] All non-H atoms were refined anisotropically. All H atoms could be located in a Fourier difference synthesis. They were placed at calculated idealized positions and refined as riding using SHELXL-2018/1 default values, except for those of the N–H and O–H groups that where fully

refined isotropically. A summary of the data collection and refinement details is given in Table 1. Crystallographic figures and tables (see Supporting Information Tables S3 to S11) were produced using PLATON.[30] A CIF file containing supplementary crystallographic data was deposited at the Cambridge Crystallographic Data Centre with reference CCDC 1991780.

Table 1. Summary of X-ray data collection and refinement parameters (polymorph I).

	5-acetic acid hydantoin
Chemical formula	$C_5H_6N_2O_2$
Colour, shape	colourless, block
Formula weight	114.11
Space group	$P2_12_12_1$
Temperature (K)	293
Cell volume (Å ^{3})	616.40(5)
Crystal system	orthorhombic
a (Å)	7.6046(4)
b (Å)	8.5920(4)
c (Å)	9.4339(5)
α (deg)	90
β (deg)	90
ɣ (deg)	90
Z	4
D_c (Mg m^{-3})	1.704
Diffractometer/scan	Bruker ApexII/ φ and *ω* scans
Radiation (Å) (graph. monochromated)	0.71073
Max. crystal dimensions (mm)	0.55×0.15×0.12
θ range (deg)	3.207-27.5
Range of *h, k, l*	–9,9; –11,11; –12;12
Reflections measured/independent	15800/1412 (R_{int}= 0.0237)
Reflections observed I >2σ	1367
Corrections applied	Absorption (Multi-scan, SADABS)
Computer programs	SHELXT-2014/5, SHELXL-2018/1, PLATON
Structure solution	Direct Methods
Data/restraints/parameters	1412/0/112
GOF	1.061
R_1 (I >2σ)	0.0252
wR_2	0.0647
Function minimized	Σ w ($\|F_o\|^2 - S\|F_c\|^2$)
Diff. density final max/min (e Å^{-3})	0.198, –0.160

All quantum chemical calculations were performed with Gaussian 09, at the DFT(B3LYP)/6–311++G(d,p) level of theory.[31-34] The computed harmonic frequencies were

scaled by a factor of 0.980, below 3400 cm^{-1}, and by 0.954, above 3400 cm^{-1}, to correct them for the effects of basis set limitations and anharmonicity. A locally modified version of the program BALGA was used to perform the normal coordinate analysis calculations.[35] The internal symmetry coordinates used in the analysis of normal modes of 5AAH are given in Table S1 (Supporting Information). Natural bond orbital (NBO) analysis was done using NBO (version 3.1), as implemented in Gaussian 09.

3. Results and discussion

3.1 Conformational landscape of 5AAH and molecular geometry

5AAH contains an asymmetric carbon (at position 5 of the hydantoin ring), and can then exist in both R and S enantiomeric configurations. The isolated molecules of the two enantiomers are, however, equivalent when one considers the properties investigated in the present study. For this reason, only the R enantiomer is considered here.

The 5AAH molecule has 3 conformationally relevant degrees of freedom, corresponding to the internal rotations about the two exocyclic C–C bonds (C5–C11 and C11–C14; see (Scheme 1) and the carboxylic C14–O16 bond. A conformational search was performed taking all these 3 internal degrees of freedom into account. A total of 36 initial structures were submitted to optimization at the DFT(B3LYP)/6–311++G(d,p) level of approximation, 18 with the carboxylic acid group in the *cis* arrangement (O=C–O–H dihedral equal to ~0º) and the other 18 possessing this group in the *trans* configuration (O=C–O–H dihedral equal to ~180º); for each of these two possibilities, 6 different initial arrangements around the C11–C14 bond were considered, each one with 3 possible orientations about the C5–C11 bond (staggered geometries). After optimization, a total of 13 minimum energy conformations were identified (Figure 1), among them 6 forms bearing a *cis* carboxylic group and the other 7 possessing this group in the *trans* configuration. Relative energies and defining geometrical data of each conformer are presented in Table 2. The equilibrium Cartesian coordinates for all minimum energy structures are provided as Supporting Information (Table S2). The geometrical parameters for the most stable conformer (*cis*-**I**) are shown in Table 3.

In terms of energy, the most relevant structural feature in the molecule of 5AAH is the conformation assumed by the carboxylic group. Following the general trend for carboxylic acids,[37-39] all conformers of 5AAH exhibiting a *cis* carboxylic moiety are lower in energy than those having this group in the *trans* orientation. The reasons for the general intrinsic higher

stability of a *cis* carboxylic group have been discussed in detail elsewhere.[38] The major factor is the existence of more favorable bond-dipole interactions in the *cis* conformation, where the polar C=O and O–H bonds show a nearly anti-parallel alignment of their dipoles, while for a *trans* carboxylic group the dipoles associated to these two bonds are approximately parallel, thus originating repulsive destabilizing interactions. Just as an illustrative example of other relevant molecular properties resulting from these different interactions in *cis* and *trans* carboxylic groups, one may mention the different characteristic C=O and O–H bond lengths in the two forms: due to their increased polarization in the *cis* conformation, both bonds are weaker (longer) in this form compared to the *trans* one. Also, the νC=O and νOH stretching frequencies (which correlate with the bond lengths) are also typically lower for *cis* than for *trans* carboxylic groups.[38-41]

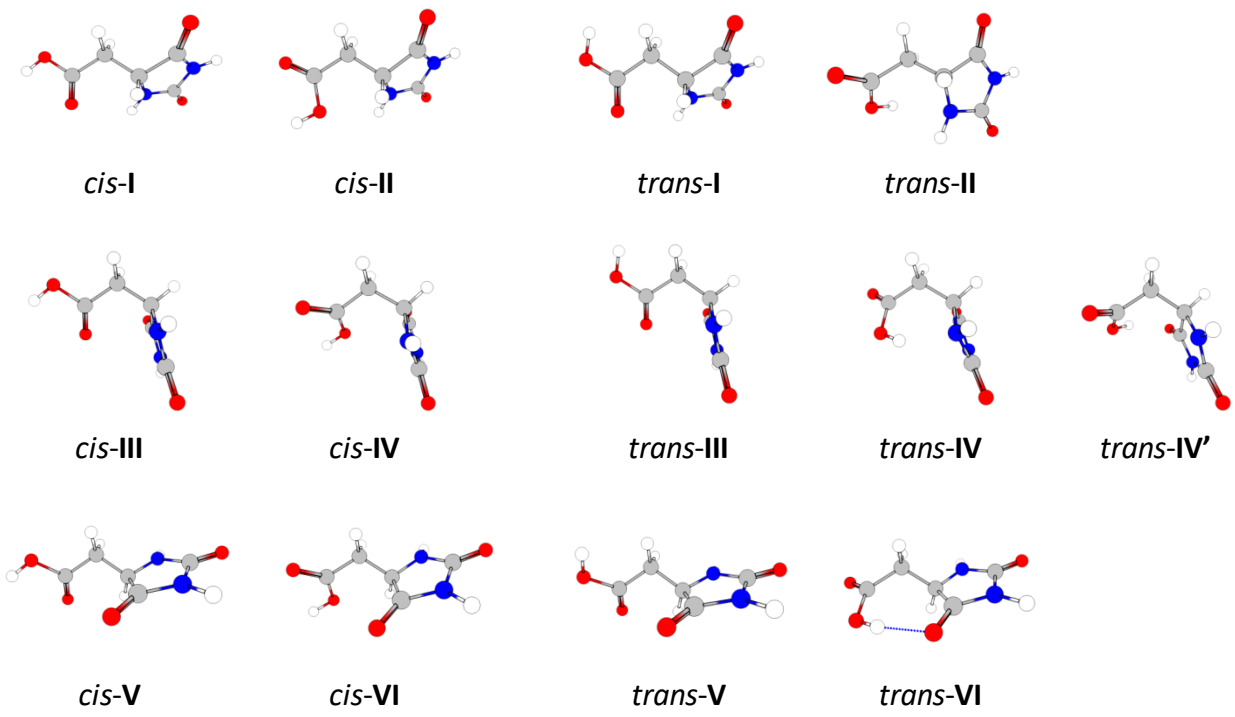

Figure 1. B3LYP/6-311++G(d,p) optimized geometries of the conformers of 5AAH (for energy data see Table 2).

The most stable 5AAH conformer is the *cis*-**I** form (see Figure 1 and Tables II and III), which shows also the usually most stable conformation around a C–C$_\alpha$(H$_2$R) bond alpha to a carboxylic group,[42,43] *i.e.*, with the C$_\alpha$–R bond (in this case the C5–C11 bond connecting the acid fragment to the hydantoin ring) eclipsing the carbonyl bond. The second most stable conformer

(*cis*-**II**; ΔE = 8.8 kJ mol^{-1}) has a similar structure to *cis*-**I**, but in this case the C5–C11 bond is eclipsing the carboxylic C–O(H) bond. In both *cis*-**I** and *cis*-**II** conformers the C4–C5 bond of the hydantoin ring is anti-periplanar relatively to the C11–C14 bond, so that the C14–C11–C5–C4 dihedral angle is ~180º. The remaining four *cis* 5AAH conformers (*cis*- **III** to **VI**) can be grouped in two pairs: in each pair (**III** and **IV**; **V** and **VI**) the conformers share a common arrangement of the hydantoin fragment and correspond to the two alternative arrangements of the acetic acid moiety (see Figure 1). In each pair, the conformer with the acetic acid fragment adopting the same conformation as in conformer *cis*-**I** is the most stable form (**III** *vs*. **IV**, and **V** *vs.* **VI**; see also Table 2), In fact, forms **III** and **V**, which are in this regard the analogous of conformer *cis*-**I**, have similar energies (12.2 and 13.4 kJ mol^{-1}, respectively) and are lower in energy than forms **IV** and **VI** (analogous to *cis*-**II**, with energies of 15.0 and 16.5 kJ mol^{-1}, respectively), indicating that for the *cis*-type conformers of 5AAH the relative importance of the conformations defined by the two conformationally relevant additional torsional coordinates (after that defining the conformation within the carboxylic group, i.e., the internal rotation around the C14–O16 bond) follows the order: C11–C14 (arrangement of the acetic acid moiety) > C5–C11 (arrangement of the hydantoin ring).

Table 2. DFT(B3LYP)/6-311++G(d,p) calculated relative electronic energies (ΔE), zero-point corrected electronic energies (ΔE(0)), Gibbs energies (at T= 298.15 K; ΔG^{o}) and conformation defining dihedral angles for the different conformers of 5AAH. [a]

Conformer	ΔE	ΔE(0)	ΔG^{o}	$H_{10}C_5C_{11}C$	CCC=O	O=COH
cis-**I**	0.0	0.0	0.0	-59.1	-3.8	-0.4
cis-**II**	8.8	8.5	6.9	-57.3	175.6	-0.4
cis-**III**	12.2	11.7	12.0	177.0	-18.0	-1.3
cis-**IV**	15.0	14.8	14.7	-168.4	130.0	-1.0
cis-**V**	13.4	13.4	12.8	38.7	-36.8	1.2
cis-**VI**	16.5	16.2	16.1	51.2	138.4	-3.5
trans-**I**	22.9	22.1	22.0	-58.4	-4.0	179.6
trans-**II**	35.0	35.4	34.4	-61.2	96.5	-178.8
trans-**III**	39.3	37.6	38.0	176.1	-14.0	-179.9
trans-**IV**	35.6	37.1	39.1	-179.2	-144.3	-179.9
trans-**IV'**	31.1	31.5	32.5	176.4	108.2	-179.9
trans-**V**	37.8	37.2	35.6	35.1	-45.3	173.6
trans-**VI**	19.0	20.2	22.5	37.8	129.4	179.7

[a] Energies in kJ mol^{-1}; angles in degrees. See Figure 1 for drawings of the conformers and Scheme 1 for atom numbering.

The *trans* conformers have structures that can be considered counterparts of those of the *cis* forms, the main difference being the conformation of the carboxylic group itself. The numbering scheme used here to designate the conformers reflects this fact. However, the following points should be noted: *(i)* as a general rule, the *trans* conformers that have an arrangement of the acetic acid fragment similar to *cis*-**II**, have more distorted geometries than those with the acetic acid fragment in a conformation similar to that observed in *cis*-**I**, with the C5–C11–C14=O dihedral angle showing values differing more from 180º than in the case of the *cis* conformers (see Table 2); essentially this results from specific intramolecular interactions between the OH fragment and the hydantoin ring (either repulsive of attractive in nature), which are pointing to each other in these conformers; on the other hand, the *trans* conformers which have an arrangement of the acetic acid fragment similar to *cis*-**I** have comparable conformational parameters to those of the corresponding *cis* forms; *(ii)* for the specific case of conformer *trans*-**VI**, the relative orientation of the acid fragment and hydantoin ring is such that an intramolecular H-bond is established between the OH group and the ring carbonylic oxygen atom O9 (see Figure 1); the existence of this intramolecular interaction (calculated H17···O9 and O16···O9 distances and O16–H17···O9 angle: 1.776 Å, 2.741 Å and 166.2º, respectively) considerably reduces the energy of the *trans*-**VI** conformer (19.0 kJ mol^{-1}), making it the most stable *trans* conformer (the relative energies of all other *trans* conformers but *trans*-**I** are over 31 kJ mol^{-1}; Table 2); (iii) two *trans* conformers were located that can be correlated with *cis*-**IV**, differing from one another essentially in the orientation of the acetic acid fragment (defined by the C5–C11–C14=O dihedral angle), which points to opposite sides of the molecule (see Figure 1); the appearance of the "extra"-minimum is also a consequence of the proximity of the OH group and the hydantoin ring in *trans* conformers exhibiting an arrangement of the acetic acid fragment of the same type of *cis*-**II**, specifically the possibility of establishment of attractive interactions between the OH group and either O9 (in conformer *trans*-**IV'**) or N1 (in *trans*-**IV**); in conformer *cis*-**IV**, these interactions are replaced by repulsive interactions between the lone electron pairs of the carboxylic O15 atom and the hydantoin O9/N1 atoms.

To evaluate the effects of the acetic acid substituent on the hydantoin ring, the structure of the most stable conformer *cis*-**I** will here be taken into account. The calculated geometry for this conformer is compared with that obtained at the same theoretical level for the parent hydantoin[2] in Table 3. The geometrical parameters of the two molecules are in general very similar, showing that the effects of the substituent present in 5AAH on the structure of the ring are not very strong.

However, some structural effects due to the presence of the acetic acid group in 5AAH (*cis*-**I**) can still be noticed, resulting from specific interactions between *(i)* the positively charged

hydrogen atoms H12/H13 and the closely located negatively charged O9, and *(ii)* H6 and O15. The first interaction leads to increase the polarization of the C4=O9 bond in 5AAH and, consequently to increase its bond length (1.208 Å, compared to 1.206 Å in hydantoin). This increase in the C4=O9 bond length in 5AAH makes this molecule to show the reverse trend observed in both hydantoin and 1-methyl hydantoin molecules[2,3] in relation to the relative lengths of the two hydantoin moiety carbonyl bonds (C4=O9 and C2=O7). In these last two molecules, the bond length of the carbonyl group C2=O7, bonded to two nitrogen atoms, is longer than that of the carbonyl group C4=O9, which is connected to a single nitrogen atom, in consonance with the expected larger total π electron delocalization from the nitrogen atoms to O7, compared to O9. In 5AAH, the C4=O9 bond is slightly longer than the C2=O7 one (1.208 *vs.* 1.207 Å). Furthermore, the existence of the (H12/H13)···O9 attractive interaction leads also to a reduction of the C5C4=O9 angle from 127.1º to 126.7º (the fact that the C5–C4 bond increases somewhat in going from hydantoin to 5AAH is explained below, and has a different origin).

As it could be expected, more significant changes result from the interaction in 5AAH between H6 and O15. To allow for a better interaction geometry, the N1–C5 bond elongates (from 1.451 from 1.455 Å), the C5N1H6 angle reduces from 125.8º to 122.4º and the geometry at the N1 atom considerably pyramidalizes [the H6-(N1C5C2) dihedral reduces from 175.7º to 158.0º].

In spite of the above noticed geometrical differences, the most relevant geometric features shown by 5AAH closely follow the trends described before for the parent hydantoin [2] (and also for 1-MH:[3]

- The ring C_{sp2}–N bond lengths increase as C2–N3 > C4–N3 > C2–N1 (1.415, 1.374, 1.370 Å, respectively), indicating a larger N-to-O electron delocalization within the N1–C2=O7 moiety, *i.e.*, when the nitrogen atom donates only to one oxygen atom. In turn, the minimum N-to-O electron charge donation takes place within the N3–C2=O7 fragment, since the N3 atom donates electron charge to both O7 and O9, and, because O7 has another donor (N1), N3 donates electron charge mostly to O9.

- The C4–C5 bond length (1.539 Å) is noticeably longer than a characteristic C_{sp3}–C_{sp2} bond length (~1.50 Å),[44] showing that the substituent linked to the C5 atom reduces the π delocalization in this region of the molecule. Interestingly, the calculated C4–C5 bond length has the same value as found previously for 1-methyl hydantoin,[3] while, as it could be expected, it is considerably longer than for the unsubstituted hydantoin (1.534 Å).[2]

Table 3. DFT(B3LYP)/6-311++G(d,p) calculated and available experimental geometrical parameters for conformers *cis*-**I** and *trans*-**III** of 5AAH (and parent hydantoin).[a]

Parameter	Calculated			Experimental[b]	
	cis-**I**	Hydantoin[2]	*trans*-**III**	*trans*-**III**	*trans*-**III**[36]
Bond length/ Å					
N1–C2	1.371	1.370	1.377	1.336(2)	1.341(3)
C2–N3	1.415	1.413	1.408	1.389(2)	1.381(2)
C2=O7	1.207	1.207	1.206	1.229(2)	1.233(3)
N3–C4	1.374	1.378	1.373	1.362(2)	1.363(3)
C4–C5	1.539	1.534	1.543	1.524(2)	1.529(3)
C4=O9	1.208	1.206	1.206	1.212(2)	1.219(2)
C5–C11	1.527		1.532	1.518(2)	1.523(3)
C11–C14	1.510		1.525	1.506(2)	1.502(3)
C14–O16	1.340		1.359	1.329(2)	1.337(3)
C14–O15	1.208		1.197	1.205(2)	1.210(3)
N1–C5	1.455	1.451	1.452	1.450(2)	1.454(3)
N1–H6	1.009	1.006	1.008	0.83(3)	0.86(3)
N3–H8	1.010	1.009	1.009	0.91(3)	0.91(2)
C5–H10	1.096	1.094	1.098	0.98	1.000
C11–H12	1.095		1.096	0.97	0.990
C11–H13	1.094		1.095	0.97	0.990
O16–H17	0.970		0.965	0.80(3)	1.02(3)
Bond angle/ º					
C5N1C2	113.0	113.3	112.8	112.5(1)	112.6(2)
N1C2N3	105.4	105.3	105.7	107.7(1)	107.6(2)
C2N3C4	113.5	113.7	113.5	111.7(1)	111.8(2)
N3C4C5	105.5	105.3	105.5	106.6(1)	106.9(2)
C4C5N1	102.1	102.4	102.0	101.2(1)	100.7(2)
N1C2=O7	129.0	128.8	128.2	127.1(1)	126.8(2)
N3C2=O7	125.6	125.9	126.1	125.2(1)	125.5(2)
N3C4=O9	127.8	127.6	128.3	125.8(1)	125.9(2)
C5C4=O9	126.7	127.1	126.1	127.5(1)	127.2(2)
C4C5C11	111.8		113.0	115.2(1)	115.3(2)
N1C5C11	114.4		115.5	114.9(1)	114.7(2)
C5C11C14	111.8		113.9	113.7(1)	113.8(2)
C11C14O16	111.7		115.2	116.3(1)	116.1(2)
C11C14=O15	125.3		124.5	123.8(1)	123.9(2)
O16C14=O15	123.0		120.3	119.9(1)	119.9(2)
C5N1H6	122.4	125.8	124.3	126(1)	127(2)
C2N1H6	120.8	120.8	119.0	121(1)	120(2)
C4N3H8	124.4	124.3	124.0	126(1)	125(2)
C2N3H8	122.1	122.0	121.9	122(1)	123(2)
C4C5H10	107.8	109.4	106.8	108.4	108.6
N1C5H10	111.0	113.2	111.4	108.4	108.6
C11C5H10	109.3		107.8	108.4	108.6
C5C11H12	110.9		108.0	108.8	108.8
C5C11H13	109.9		109.6	108.8	108.8
C14C11H12	108.2		107.8	108.8	108.8
C14C11H13	109.3		110.2	108.8	108.8
H12C11H13	106.6		106.9	107.7	107.6
C14O16H17	107.7		111.2	110(2)	110(2)
Dihedral angle/ º					
C5N1C2N3	-6.9	1.3	-4.8	-4.1(2)	-4.4(2)
N1C2N3C4	3.2	-0.7	0.1	0.4(2)	0.3(2)
C2N3C4C5	1.5	0.0	4.2	3.2(2)	3.6(2)
N3C4C5N1	-5.2	0.7	-6.4	-5.1(2)	-5.6(2)
C4C5N1C2	7.6	-1.4	7.0	5.7(2)	6.1(2)
H6-(N1C5C2)	158.0	-175.7	157.6	174.9	175.0
O7=(C2N1N3)	-179.4	-179.9	179.2	179.6(2)	179.7(2)
H8-(N3C2C4)	-179.3	179.9	-171.7	-179.0	-179.5
O9=(C1N3C5)	-179.9	-179.9	177.9	176.9(3)	176.5(2)
H10C5C11C14	-59.1		176.1	175.3	175.3
C5C11C14=O15	-3.8		-14.0	-15.7(2)	-16.0(3)
O15=C14O16H17	-0.4		-179.9	-179.7(2)	-180.0(2)

[a] See Figure 1 for drawings of the conformers and Scheme 1 for atom numbering. [b] Uncertainties (in parentheses) are given in units of the last digit. The experimental data for *trans*-III from[36] were taken at 173(2) K, those from our work were obtained at 293(2) K.

Following also the trend already noticed before for the parent hydantoin and both 1-methyl and 5-methyl hydantoins,[2-4] the ring internal angles with a nitrogen atom in the apex (C4–N3–C2 and C5–N1–C2) are much larger (around 113º) than those with carbon atoms in the apex (N1–C2–C3, N1–C5–C4 and N3–C4–C5; ~102-106º), pointing to relatively different *s vs. p* composition of the hybrid orbitals of the N and C atoms used to make the ring bonds.

3.2 Natural Bond Orbital (NBO) analysis

As in our previous studies on hydantoin and 1- and 5-methyl substituted hydantoins[2-4] we used the NBO method to investigate in more detail the electronic structure of 5AAH, in particular to look to the specific characteristics of its σ and π electronic systems.

The NBO atomic charges are given in Table 4. The total charges of the two nitrogen atoms and of the four oxygen atoms are negative, because they are more electronegative than the carbon atoms (for O16 also H17) to which they are connected. In a similar way, carbon atoms C2, C4 and C14 that are bonded to more electronegative nitrogen or oxygen atoms have positive total charges, opposing to C5 and C11 that show a negative total charge, since they are connected to hydrogen atoms. C11 is connected to two hydrogen atoms and is more negative than C5, which is bonded only to one hydrogen atom.

Better than the total charges, the NBO charges' partition in terms of the electronic σ and π systems brings to light some considerably more interesting details of the electron distribution in the molecule.

The first observation is that, despite the nitrogen atoms present a negative total charge, they have a positive π charge, in consonance with the mesomeric structures II, III and IV drawn in Scheme 2. N3 has more positive π charge than N1, in consonance with the fact that it shows a positive charge in mesomeric structures III and IV, whereas N1 shows only a positive charge in II. The relative values of the π charges of the nitrogen atoms agree also with the relative lengths of the C_{sp2}–N bonds. As point out above, the structural results indicate a maximum N-to-O electron delocalization in the N1–C2=O7 fragment. In consonance with this result, the positive π charge of the N1 atom (+0.246 *e*), which is essentially a consequence from the π delocalization to O7 (see Scheme 2), is noticeably larger than half of the charge of N3 (+0.145 *e*), which donates π electron charge to both O7 and O9.

An identical reasoning can be used to explain the relative π charges of the two oxygen atoms bound to the ring: O7 shows a negative charge in two mesomeric structures (II and IV) and has a more negative π charge than O9, which shows a negative charge only in III. The σ charges of these two oxygen atoms are substantially less negative than the π charges and, very interestingly, have opposite relative values (the O9 σ charge is more negative than the O7 σ charge; Table 4). This shows that, in comparison with C4=O9, the larger C2=O7 π bond

polarization towards the oxygen atom reduces the trend for the corresponding σ bond to be polarized in the same direction.

Table 4. NBO atomic charges for 5-AAH (*cis*-**I**), obtained from the B3LYP/6-3111++G(d,p) calculations.[a]

	NBO charges		
Atom	Total	σ	π
N1	–0.799	–1.045	0.246
C2	0.981	0.744	0.236
N3	–0.825	–1.116	0.291
C4	0.805	0.559	0.245
C5	–0.131	0.089	–0.221
H6	0.461	-	-
O7	–0.649	–0.132	–0.517
H8	0.466	-	-
O9	–0.606	–0.137	–0.469
H10	0.278	-	-
C11	–0.583	–0.348	–0.237
H12	0.283	-	-
H13	0.291	-	-
C14	0.920	0.629	0.290
O15	–0.644	–0.121	–0.523
O16	–0.739	–0.808	0.069
H17	0.492	-	-

[a] Charges in units of electron (e = 1.60217646 x 10^{-19} C); See Scheme 1 for atom numbering.

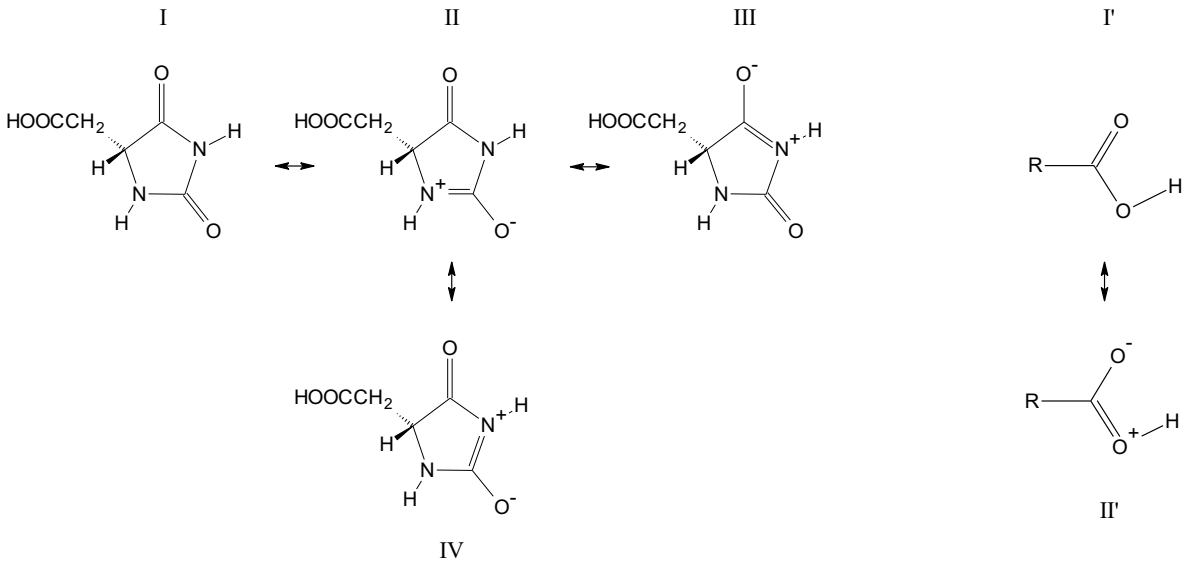

Scheme 2. I, I': Dominant canonic forms for 5AAH hydantoin ring and carboxylic acid fragment. II, III and IV: mesomeric structures assuming delocalization of π electrons in the NCO ring moieties of the molecule; II': mesomeric structure assuming delocalization of π electrons within the carboxylic acid fragment. R= hydantoin ring.

Both the total and σ/π NBO charge partition for the carbonyl oxygen of the acetic acid fragment (O15) closely follows that of the two carbonyl oxygen atoms connected to the hydantoin ring. In turn, the carboxylic acid O16 atom shows a completely different pattern: the total and σ charges are strongly negative, as it could be expected, but the π charge is slightly positive, which is in consonance with the relevance of the mesomeric structure II' shown in Scheme 2 to the electronic structure of this fragment.

Table 5 presents the most relevant NBO interactions expressed in terms of the orbital interaction energies, $-E(2)$], which provide also information on the relative importance of the mesomerism within the different fragments of the 5AAH molecule, as well as on other important intramolecular interactions.

Table 5. Stabilization energies for selected NBO pairs as given by second order perturbation theory analysis of the Fock matrix in the NBO basis for 5AAH obtained from the B3LYP/6-311++G(d,p) calculations. [a]

Pair name	Donor NBO	Acceptor NBO	–E(2) Energy (kcal mol^{-1})
A	LP (N3)	π* (C4=O9)	81.68
B	LP (N1)	π* (C2=O7)	81.53
C	LP2 (O16)	π*(C14=O15)	72.50
D	LP (N3)	π*(C2=O7)	63.97
E	LP2 (O15)	σ*(C14–O16)	49.45
F	LP2 (O7)	σ*(C2–N3)	45.24
G	LP2 (O9)	σ*(N3–C4)	41.32
H	LP2 (O7)	σ*(N1–C2)	38.61
I	LP2 (O9)	σ*(C4–C5)	30.69
J	LP1 (O7)	RY(C2)	28.91
K	LP1 (O9)	RY(C4)	27.74
L	LP1 (O15)	RY(C14)	26.90
M	LP2 (O15)	σ*(C11–C14)	24.97

[a] See atom numbering in Scheme 1. LP, lone electron pair orbital. RY, Rydberg type orbital. CR, core orbital.

As it is shown in this Table, the most relevant NBO interactions, A, B, C and D, involve electron charge transfer from the lone electron pair (LP) of the nitrogen atoms (A, B, D) or the acid oxygen O16 (C) to the carbonyl bonds' π anti-bonding orbitals. These interactions can be directly related with mesomeric structures II, III, IV and II' presented in Scheme 2. For N1, the charge transfer is only to the π*(C2=O7) orbital, while N3 donates electronic charge to both π*(C2=O7) and π*(C4=O9) orbitals. The total electronic charge transferred from the N1 and N3 atoms to the π*(C2=O7) anti-bonding orbital is then considerably larger than that resulting from the single interaction associated with the π*(C4=O9) anti-bonding orbital. The NBO interaction results then reinforce the conclusions extracted from the structural data, *e.g.*, those explaining the relative lengths of the different C_{sp2}–N bonds (C2–N1 < C4–N3 < C2–N3) pointed out above,

and are also in agreement with the more negative π charge predicted for O7 (–0.517 *e*), compared to O9 (–0.469 *e*).

NBO interactions E-M represent other types of intramolecular interactions: *(i)* interactions designated as E-I and M occur between the non-bonded electron pair (LP2; σ) of O7, O9 and O15 atoms and the anti-bonding σ* orbitals of the neighbor bonds. They are related with the previously described electron back-donation effect involving carbonyl oxygen atoms[45-47] that explains, for example, the unusually long C–H bond length in aldehydes and derivatives of formic acid, and that reflects also in the uncommonly low ν(C–H) stretching vibrational frequency in these types of molecules. *(ii)* The J, K and L NBO orbital interactions relate with the electronic charge transfer from the second non-bonded electron pair (LP1; σ) of the carbonyl oxygen atoms O7, O9 and O15 to a Rydberg orbital of the corresponding carbon atom, and are connected with effects associated with the carbonyl bond polarization; these effects work as moderators of the σ polarization of the carbonyl bonds, to compensate the effects of the increased π polarization due to the interactions A-D.

The *s vs. p* composition of the hybrid NBO's of the ring atoms (see Table 6) allows explaining why the internal angles of the ring are significantly larger when they have a nitrogen atom in the apex (C4–N3–C2 and C2–N1–C5) than when they have a carbon atom occupying this position (N1–C2–N3, N3–C4–C5 and N1–C5-C4). As already mentioned, this observation points to different *s vs. p* composition of the hybrid orbitals of the C and N atoms that are used to from the ring bonds, since a smaller *p* contribution to the orbital can be correlated with a larger angle. [48,49] Accordingly, the average *p* contribution to the hybrid orbitals used to establish the ring bonding NBOs by the nitrogen atoms N1 and N3 is smaller than that used by the carbon atoms C2, C4 and C5.

3.3 IR spectrum of matrix-isolated 5AAH

The infrared spectrum of monomeric 5AAH isolated in an argon matrix (T= 10 K) is shown in Figure 2, where it can be compared with the B3LYP/6–311++G(d,p) calculated IR spectrum of conformer *cis*-**I**, which could be anticipated to be the sole conformer of 5AAH trapped in the cryogenic matrix. Indeed, the expected population of *cis*-**I** in the gas phase prior to deposition, calculated based on the B3LYP Gibbs energies at 298 K (see Table 2) and assuming the Boltzmann distribution, is ~93%. The predicted room temperature gas phase populations for all other conformers but conformer *cis*-**II** are smaller than 0.8%, *i.e.*, below the detection limit of the experimental technique, except that of conformer *cis*-**II** that is ~6% and, in principle, large enough to allow for its experimental detection. However the energy barrier separating *cis*-**II** from the most stable *cis*-**I** conformer is very small (~5 kJ mol^{-1}; see Figure 3)

Table 6. Selected NBOs for 5-HAA obtained from the B3LYP/6-311++G(d,p) calculations.

Bond orbital [a]	Occupancy [b] (e)	Coefficients (%) [c]		Description [d]
$T(A\text{-}B)$		A	B	
σ (N1-C2)	1.99093	63.43	36.57	0.7965 $sp^{1.89}$ + 0.6047 $sp^{2.00}$
σ (N1-C5)	1.98449	61.87	38.13	0.7865 $sp^{2.05}$ + 0.6175 $sp^{3.78}$
σ (N1-H6)	1.98765	73.43	26.57	0.8569 $sp^{2.28}$ + 0.5155 s
σ (C2-N3)	1.98788	35.15	64.85	0.5929 $sp^{2.29}$ + 0.8053 $sp^{1.98}$
σ (C2=O7)	1.99728	34.56	65.44	0.5878 $sp^{1.83}$ + 0.8090 $sp^{1.41}$
π (C2=O7)	1.99575	28.41	71.59	0.5330 p + 0.8461 p
σ (N3-C4)	1.99030	64.45	35.55	0.8028 $sp^{1.80}$ + 0.5962 $sp^{2.29}$
σ (N3-H8)	1.98853	73.61	26.39	0.8580 $sp^{2.26}$ + 0.5137 s
σ (C4-C5)	1.97992	47.52	52.48	0.6893 $sp^{1.83}$ + 0.7245 $sp^{3.05}$
σ (C4=O9)	1.99747	34.27	65.73	0.5854 $sp^{1.98}$ + 0.8107 $sp^{1.34}$
π (C4=O9)	1.99442	30.94	69.06	0.5562 p + 0.8310 p
σ (C5-H10)	1.97281	64.12	35.88	0.8007 $sp^{2.88}$ + 0.5990 s
σ (C5-C11)	1.97737	50.67	49.33	0.7118 $sp^{2.49}$ + 0.7024 $sp^{2.81}$
σ (C11-H12)	1.97294	64.08	35.92	0.8005 $sp^{3.12}$ + 0.5993 s
σ (C11-H13)	1.97184	64.46	35.54	0.8029 $sp^{3.06}$ + 0.5962 s
σ (C11-C14)	1.98378	51.66	48.34	0.7188 $sp^{3.01}$ + 0.6952 $sp^{1.50}$
σ (C14=O15)	1.99831	33.09	66.91	0.5752 $sp^{2.09}$ + 0.8180 $sp^{1.32}$
π (C14=O15)	1.99351	29.80	70.20	0.5459 p + 0.8378 p
σ (C14-O16)	1.99691	30.86	69.14	0.5555 $sp^{2.63}$ + 0.8315 $sp^{1.87}$
σ (O16-H17)	1.98843	74.99	25.01	0.8660 $sp^{3.67}$ + 0.5001 s
Cr (N1)	1.99905			s
Cr (C2)	1.99944			s
Cr (N3)	1.99894			s
Cr (C4)	1.99912			s
Cr (C5)	1.99872			s
Cr (O7)	1.99959			s
Cr (O9)	1.99959			s
Cr (C11)	1.99868			s
Cr (C14)	1.99919			s
Cr (C15)	1.99960			s
Cr (O16)	1.99963			s
LP (N1)	1.80944			p
LP (N3)	1.73025			p
LP1 (O7)	1.97580			$sp^{0.73}$
LP2 (O7)	1.85580			p
LP1 (O9)	1.97770			$sp^{0.76}$
LP2 (O9)	1.87577			p
LP1 (O15)	1.97535			$sp^{0.76}$
LP2 (O15)	1.87398			p
LP1 (O16)	1.97725			$sp^{1.29}$
LP2 (O16)	1.86006			p
Ry* (C2)	0.02137			$sp^{13.23}$
Ry* (C4)	0.01991			$sp^{9.07}$
σ* (N1-C2)	0.06854	36.57	63.43	0.6047 $sp^{1.89}$ – 0.7965 $sp^{2.00}$
σ* (N1-C5)	0.01882	38.13	61.87	0.6175 $sp^{2.05}$ – 0.7865 $sp^{3.78}$
σ* (N1-H6)	0.01197	26.57	73.43	0.5155 $sp^{2.28}$ – 0.8569 s
σ* (C2-N3)	0.08288	64.85	35.15	0.8053 $sp^{2.29}$ – 0.5929 $sp^{1.98}$
σ* (C2=O7)	0.01368	65.44	34.56	0.8090 $sp^{1.83}$ – 0.5878 $sp^{1.41}$
π* (C2=O7)	0.26954	71.59	28.41	0.8461 p – 0.5330 p
σ* (N3-C4)	0.07090	35.55	64.45	0.5962 $sp^{1.80}$ – 0.8028 $sp^{2.29}$
σ* (N3-H8)	0.01148	26.39	73.61	0.5137 $sp^{2.26}$ – 0.8580 s
σ* (C4-C5)	0.06305	52.48	47.52	0.7245 $sp^{1.83}$ – 0.6893 $sp^{3.05}$
σ* (C4=O9)	0.01015	65.73	34.27	0.8107 $sp^{1.98}$ – 0.5854 $sp^{1.34}$
π (C4=O9)	0.18639	69.06	30.94	0.8310 p – 0.5562 p
σ* (C5-H10)	0.01929	35.88	64.12	0.5990 $sp^{2.88}$ – 0.8007 s
σ* (C5-C11)	0.02177	49.33	50.67	0.7024 $sp^{2.49}$ – 0.7118 $sp^{2.81}$
σ* (C11-H12)	0.00925	35.92	64.08	0.5993 $sp^{3.12}$ – 0.8005 s
σ* (C11-H13)	0.00906	35.54	64.46	0.5962 $sp^{3.06}$ – 0.8029 s
σ* (C11-C14)	0.05088	48.34	51.66	0.6952 $sp^{3.01}$ – 0.7188 $sp^{1.50}$
σ* (C14=O15)	0.02138	66.91	33.09	0.8180 $sp^{2.09}$ – 0.5752 $sp^{1.32}$
π* (C14=O15)	0.16737	70.20	29.80	0.8378 p – 0.5459 p
σ* (C14-O16)	0.08277	69.14	30.86	0.8315 $sp^{2.63}$ – 0.5555 $sp^{1.87}$
σ* (O16-H17)	0.01103	25.01	74.99	0.5001 $sp^{3.67}$ – 0.8660 s

[a] See atom numbering in Scheme 1. Type of orbital (T): Cr, core orbital; LP, lone electron pair orbital; Ry*, Rydberg orbital. [b] Occupancy is given with an exaggerated accuracy, as in the Gaussian output file. [c] The A and B values correspond to the contributions of the atomic orbitals of the two atoms forming a bond (by order of appearance in the corresponding entry in the first column) for the NBO orbitals, extracted from the polarization coefficients given in the description of the NBO orbitals. [d] The presented description is made in the space of the input atomic orbitals, as given by 6-311++G(d,p) basis set used in the calculations.

Under these conditions, it can be anticipated that *cis*-**II** should promptly convert to *cis*-**I** upon matrix deposition, since conformational cooling leading to conversion, at the time of matrix deposition, of higher-energy conformers into lower-energy forms from which they are separated by small energy barriers (of a few kJ mol^{-1}) is a well-known common phenomenon.[50,51] The good agreement between the experimentally observed IR spectrum of the as-deposited 5AAH argon matrix and the calculated spectrum for conformer *cis*-**I** (see Figure 2) confirms that only this form is present in detectable amounts in the cryogenic matrix.

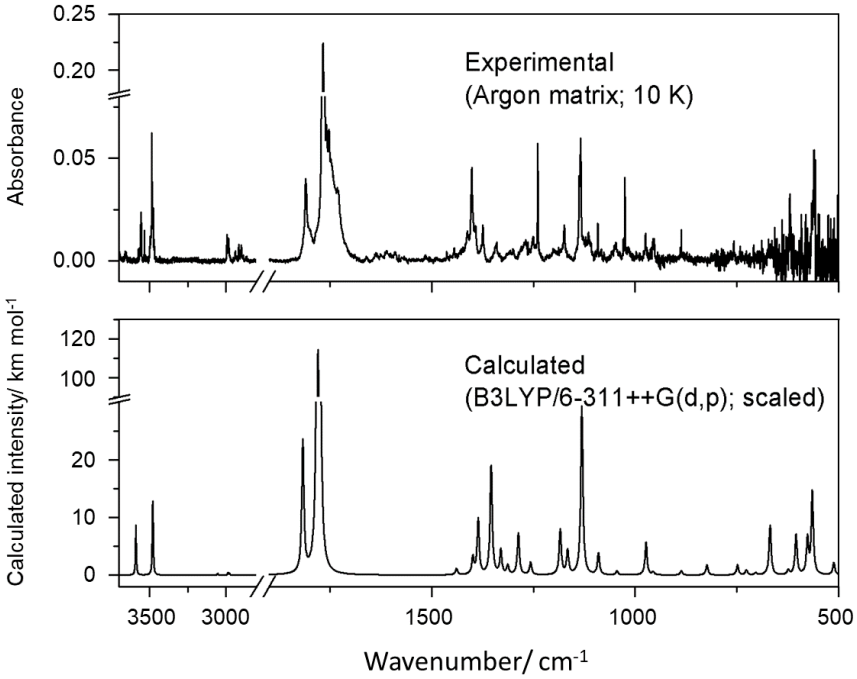

Figure 2. Experimental infrared spectrum of monomeric 5AAH isolated in an argon matrix at 10 K (*top*) and simulated spectrum of conformer *cis*-I, using Lorentzian functions centered at the scaled B3LYP/6-311++G(d,p) calculated wavenumbers, with calculated intensities corresponding to areas below the bands (*bottom*).

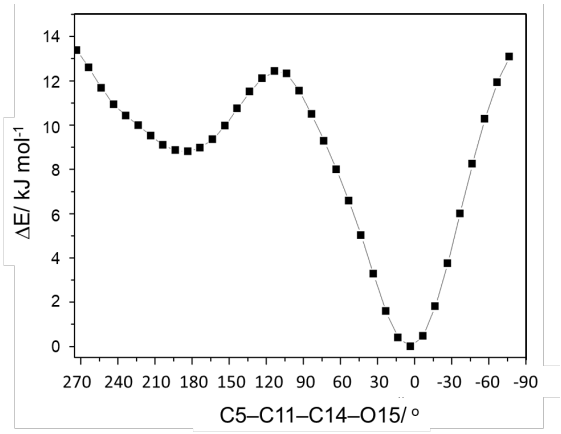

Figure 3. B3LYP/6-311++G(d,p) calculated potential energy profile for interconversion between conformers *cis*-**I** and *cis*-**II**.

The calculated normal modes were characterized in terms of their potential energy distributions (PED), which are given together with the proposed assignments in Table 7. Globally, the experimental and calculated spectra agree very well. The most intense band is ascribable to the anti-symmetric ring carbonyl stretching vibration ($\nu(C=O)_{as}$), being observed at 1768 (calculated, 1775 cm^{-1}). As reported before for the parent hydantoin and its 1-methyl and 5-methyl substituted derivatives [2-4] this band has a satellite band at ~1753 cm^{-1} (appearing as a shoulder of the main band) which shall be assigned to the first overtone of the $\nu(C_{11}\text{-}C_{14})$ vibration (whose fundamental appears at 889/886 cm^{-1}) enhanced by Fermi resonance interaction with $\nu(C=O)_{as}$. The symmetric ring carbonyl stretching vibration ($\nu(C=O)_{s}$) is observed at 1810 cm^{-1} (calculated at 1817 cm^{-1}), while the substituent $\nu(C_{14}=O)$ carbonyl stretching mode gives rise to the band observed at 1752 cm^{-1} (calculated 1775 cm^{-1}) which appears also overlapped with the most intense band due to $\nu(C=O)_{as}$. The out-of-plane bending modes of the carbonyl groups of the hydantoin ring ($\gamma(C_2=O)$ and $\gamma(C_4=O)$) are observed as matrix-site split doublets at 757/741 and 709/707 cm^{-1}, in good agreement with the calculated values (748, 703 cm^{-1}), while the equivalent vibration of the substituent ($\gamma(C_{14}=O)$) is observed at 512/510 cm^{-1} (calculated value: 511 cm^{-1}). The order of frequencies for these 3 modes, $\gamma(C_2=O) > \gamma(C_4=O) > \gamma(C_{14}=O)$, reflects the greater rigidity of the N–C2=O7–N fragment in relation to out-of-plane deformations, compared to the N–C4=O9–C fragment, and of this latter compared to the substituent group, due to the presence of two NH/C=O interactions in the first fragment, one in the second, and none in the substituent.

The NH stretching vibrations are observed as a pair of overlapped bands at 3485 and 3477 cm^{-1} ($\nu(N_1H)$ and $\nu(N_3H)$, respectively; predicted values: 3482 and 3479 cm^{-1}). The relative values of the frequencies of the two NH stretching vibrations correlate with the lengths of the two bonds, the higher the frequency the shorter the N–H bond (the calculated N1–H and N3–H bond lengths are 1.009 and 1.010 Å, respectively; Table 3). The $\delta(N_1H)$ and $\delta(N_3H)$ in-plane bending vibrations are observed at 1340 and 1306 cm^{-1} respectively, matching fairly well the calculated values (1353 and 1330 cm^{-1}), while the corresponding out-of-plane bending vibrations ($\gamma(N_1H)$ and $\gamma(N_3H)$) are observed at 467 and 565/559 cm^{-1} as relatively high intensity. The higher frequency for the $\gamma(N_3H)$ mode reflects the fact that the N3–H moiety participates in two NH/C=O interactions, while the N1–H group is involved in only one of this type of interactions. Taken together with what has been pointed out above regarding the ring carbonyl groups, this result demonstrates that the most rigid part of the hydantoin ring in relation to out-of-plane deformation is the fragment N1–C2(=O7)– N3(H)–C4.

Table 7. Infrared spectrum of monomeric 5AAH in argon matrix (10 K) and DFT(B3LYP)/6-311G++(d,p) calculated infrared spectrum and potential energy distributions (PED).[a]

Experimental (Ar matrix; 10 K)	Calculated		
Wavenumber[b]	Wavenumber[c]	I_{IR}[d]	PED[e] (%)
3557/3534	3590	81	ν(OH) (100)
3485	3482	40	$\nu(N_1H)$ (98)
3477	3479	100	$\nu(N_3H)$ (98)
2994	3054	3	$\nu(CH_2)_{as}$ (100)
2985	2986	4	$\nu(CH_2)_s$ (90) +ν(CH) (10)
2939/2917/2899	2978	3	ν(CH) (90) + $\nu(CH_2)_s$ (10)
1810	1817	214	$\nu(C{=}O)_s$ (80)
1767/~1753 (FR)	1781	979	$\nu(C{=}O)_{as}$ (63) + $\nu(C_{14}{=}O)$ (16)
1752	1775	376	$\nu(C_{14}{=}O)$ (70) + δ(COH) (14)
1444	1439	10	$\delta(CH_2)$ (98)
1401	1399	28	$w(CH_2)$ (46) + δ(CH) (15) + $\delta(N_1H)$ (11)
1374	1386	91	γ(CH) (56) + $w(CH_2)$ (56) + $\nu(C_5\text{-}C_{11})$ (10)
1340	1353	177	$\delta(N_1H)$ (46) + δ(CH) (15)
1306	1330	40	$\delta(N_3H)$ (58) + δ(CH) (13)
1300	1313	15	ν_3(ring) (46) + $\delta(N_3H)$ (38)
1269	1288	68	δ(COH) (55) + $\nu(C_{14}\text{-}O)$ (30)+ wCH_2) (16)
1250/1239	1257	20	ν_2(ring) (38) + δ(COH) (26)+ δ(CH) (16)
1174	1184	74	$tw(CH_2)$ (85)
n.obs.	1166	40	ν_1(ring) (68) + δ(CH) (26)
1137/1133	1131	275	$\nu(C_{14}\text{-}O)$ (55)+ δ(COH) (37) + $w(CH_2)$ (17)
1091	1090	35	$\nu(C_5\text{-}C_{11})$ (45) + ν_3(ring) (14)+ ν_2(ring) (11) + $\delta(N_1H)$ (10)
1028/1024	1044	6	$\gamma(CH_2)$ (79) + $\nu(C_{11}\text{-}C_{14})$ (11)
974	973	54	ν_5(ring) (67) + $\gamma(CH_2)$ (24)
955/953/951	955	5	γ(CH) (49) + $\nu(C_5\text{-}C_{11})$ (44)
889/886	886	7	$\nu(C_{11}\text{-}C_{14})$ (74) + δ(CCC) (20)
814/811/787	823	17	ν_4(ring) (61) + $\nu(C_{11}\text{-}C_{14})$ (14)
757/741	748	17	$\gamma(C_2{=}O)$ (86)
725	726	8	δ_2(ring) (53) + ν_2(ring) (20)
709/707	703	4	$\gamma(C_4{=}O)$ (41) + τ(OH) (23)
688/671	668	81	δ_1(ring) (44) + τ(OH) (13)
631	623	8	τ(OH) (63)
611/609	604	65	δ(CC=O) (31) + δ(CCO) (30) + δ_2(ring) (10)
581	575	58	$\delta(C_2{=}O)$ (34) + $\delta(C_4{=}O)$ (34) + $\gamma(N_3H)$ (10)
565/559	564	135	$\gamma(N_3H)$ (79) + δ(COH) (10)
512/510	511	20	$\gamma(C_{14}{=}O)$ (61) + τ (OH) (11)
467	457	49	$\gamma(N_1H)$ (72) + $\gamma(N_3H)$ (11)
433	426	58	δ(CCO) (41) + δ(CC=O) (40) + τ_1(ring) (10)
n.i.	393	10	$\delta(C_{11}(ring))$ (40) + $\delta(C_2{=}O)$ (23) + $\delta(C_4{=}O)$ (23)
n.i.	312	6	$\delta(CCO)$ (18) + $\gamma(C_{11}(ring))$ (18)
n.i.	247	5	$\gamma(C_{11}(ring))$ (40) + δ(CCC) (17)
n.i.	172	2	τ_2(ring) (63) + τ_1(ring) (27)
n.i.	139	1	δ(CCC) (33) + τ_1(ring) (19)
n.i.	74	0.1	τ_1(ring) (54) + τ_2(ring) (19))
n.i.	60	2	$\tau(C_5\text{-}C_{11})$ (88)
n.i.	39	2	$\tau(C_{11}\text{-}C_{14})$ (98)

[a] See Table S1 for the definition of coordinates and Scheme 1 for atom numbering. Abreviations: s, symmetric; as, anti-symmetric; ν, stretching; δ, in-plane bending; γ, out-of-plane bending; τ, torsion, w, wagging; tw, twisting; n.obs., not observed; n.i., not investigated; FR, Fermi resonance. [b] Wavenumbers in cm^{-1}. [c] Calculated wavenumbers are scaled. [d] IR intensities in km mol^{-1}. [d] PED's lower than 10% not shown.

The ν(OH) band is observed at 3557/3534 cm^{-1} in good agreement with the calculated value (3590 cm^{-1}), while the δ(COH) and ν(C_{14}–O) coordinates are extensively coupled as usually for carboxylic acids[40-42] (see Table 7) and give rise to the intense bands observed at 1269 and 1137/1133 cm^{-1} (predicted at 1288 and 1131 cm^{-1}, respectively). The τ(OH) torsional vibration was observed at 631 cm^{-1}, in good agreement with the calculated data (623 cm^{-1}).

The remaining vibrations give rise to bands of lower intensity and the general agreement between the experimental and calculated wavenumbers and relative intensities is also very good (see Table 7), so that their assignment was straightforward.

3.4 Thermal investigation of 5AAH

The commercially obtained compound was recrystallized from different solvents. The crystals obtained upon recrystallization from dichloromethane, acetone, water, methanol and ethanol were identical and equal to the original material (from now on designated as polymorph **I**). DSC analysis of this polymorph (Figure S1) showed that it melts at T_{fus} = (214.3 ± 0.8) ºC, with an enthalpy of fusion of $\Delta_{fus}H$ = (37.0 ± 1.5) kJ mol^{-1}. Besides the melting of the sample, no other events were observed during the heating of polymorph **I**. Recrystallization from THF and 1,4-dioxane solutions led to heterogenic polymorphic mixtures of polymorphs **I**, **II** and **III**, in the first case, and **I** and **IV** in the later. Separation of the polymorphs obtained simultaneously was not achieved, so that their characterization was only possible using microanalytical instrumental techniques, in particular micro-Raman spectroscopy and PLTM, as described below. The crystals of the polymorphs **II**-**IV** used in the PLTM experiments were gathered from the obtained polymorph mixtures and selected after their identification by taking into account their Raman spectra.

The PLTM analysis of polymorph **I** confirms the results obtained by DSC, as shown in Figure 4.1. Polymorph **II** melts at *ca.* 184-185 ºC (Figure 4.2). Like for polymorph **I**, no other events were also observed when polymorph **II** was heated from room temperature up to its melting. The same happens for polymorph **III**, whose melting takes place at *ca.* 175-178 ºC (Figure 4.3). On the other hand, polymorph **IV** undergoes a solid-solid transition (at *ca.* 180-185 ºC; Figure 5), transforming into a new polymorph (polymorph **V**) that then melts at *ca.* 198-200 ºC. The Raman spectra of polymorphs **I** to **IV** were obtained and clearly show the different nature of the different polymorphs (see Figure 6). Raman shifts of the observed bands and proposed assignments are collected in Table 8. The Raman spectrum of polymorph **V** could not be

obtained, since we were not able to isolate this form in a suitable amount for undertaking the experiments.

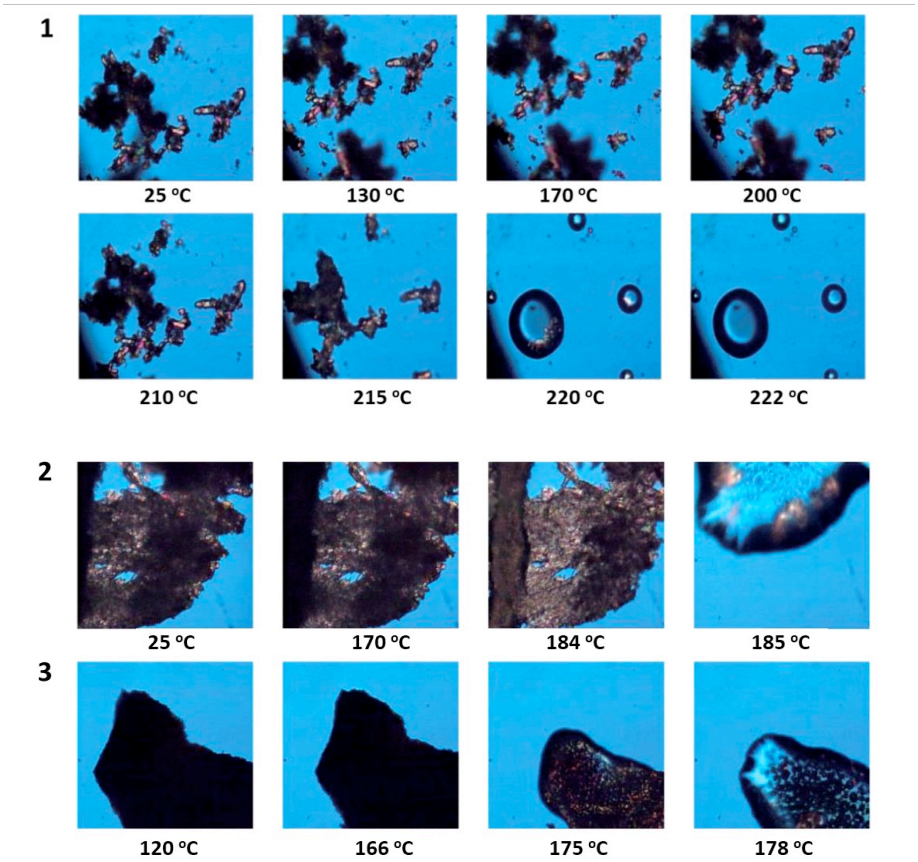

Figure 4. Polarized light thermal microscopy images collected during heating of polymorphs **I** (part 1; *top*), **II** (part 2; *middle*) and **III** (part 3; *bottom*) of 5AAH from 25 ºC to about their melting temperatures (heating rate: 10 ºC min^{-1}, amplification 200x).

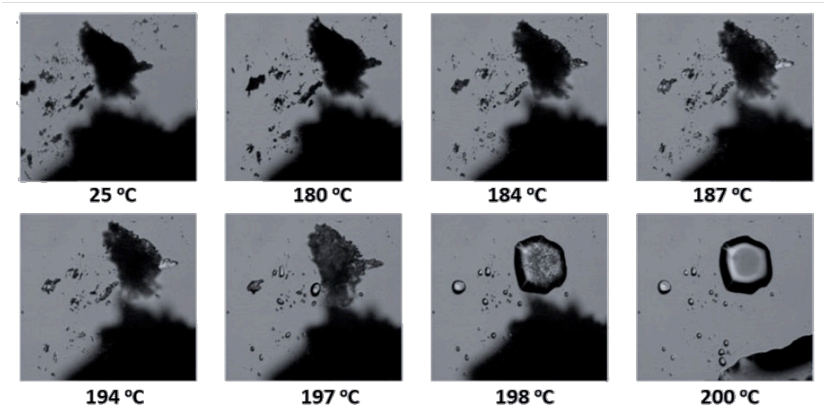

Figure 5. Polarized light thermal microscopy images collected during heating of an initial sample of polymorph **IV** of 5AAH from 25 to 200 ºC (heating rate: 10 ºC min^{-1}, amplification 200x). The **IV**→**V** solid-solid transition is observed at *ca.* 180-185 ºC, with the melting of the generated polymorph **V** being observed at *ca.* 198-200 ºC.

Table 8. Raman bands (wavenumbers; cm^{-1}) of polymorphs **I** to **IV** of 5AAH, at 25 ºC, with proposed assignments. [a]

Polymorph **I**	Polymorph **II**	Polymorph **III**	Polymorph **IV**	Assignment[b]
3347	3221	3273	3214	$\nu(N_1H)$, $\nu(N_3H)$
3194/3066	3183	3135/3030	3169	ν(OH)
2980	2983	2966/2960	2981	$\nu(CH_2)_{as}$
2945	2966/2960	2924	2940	$\nu(CH_2)_s$
2916	2938/2927/2889	2924	2914	ν(CH)
1770	1769	1761	1759	$\nu(C{=}O)_s$
1738	1732	1733	1735/ 1729	$\nu(C{=}O)_{as}$
1679	17031673	1707/1676/1634	1697	$\nu(C_{14}{=}O)$
1530			1530	$\delta(CH_2)$
1460	1483/1460	1468	1462	$w(CH_2)$
1439/1425	1439/1430	1430/1423	1434	γ(CH)
1402/1390	1405	1405/1399	1414	$\delta(N_1H)$
1358/1346	1357/1331	1358/1332	1359/1338	$\delta(N_3H)$
1314	1325	1332	1338	ν_3(ring)
1292	1293	1297/1255	1316/1264	δ(COH)
1233	1233/1225	1225	1211	ν_2(ring)
1200	1203	1203	1201	$tw(CH_2)$
n.obs.	1194	1197	1182	ν_1(ring)
1121	1123	1120	1134	$\nu(C_{14}\text{-}O)$
1049	1058	1057	1067	$\nu(C_5\text{-}C_{11})$
1032	1037	1046	n.obs.	$\gamma(CH_2)$
1022	1018	1018	1004	ν_5(ring)
937	961	960	961	γ(CH)
921/912	922/913	911/904	912	$\nu(C_{11}\text{-}C_{14})$
836	881	881/836	886	ν_4(ring)
795/789	778	778	767	$\gamma(C_2{=}O)$
765	737	752/738	739	δ_2(ring)
709	706	703	n.obs.	$\gamma(C_4{=}O)$
690/663	675	685/676	679/659	τ(OH)
640	635	635	640	δ_1(ring)
597	612	613	614	$\gamma(N_3H)$
582	562	559	559	δ(CC=O)
545	515	497	482	$\delta(C_2{=}O)$, $\delta(C_4{=}O)$
518	499	473	482	$\gamma(C_{14}{=}O$
509	475	470	482	$\gamma(N_1H)$
435	423	422	435	δ(CCO)
361	368/350	369/349	390	$\delta(C_{11}$(ring))
278/267	300	301	266	$\delta(C_2{=}O)$, $\delta(C_4{=}O)$
215/206	242	245	213	$\gamma(C_{11}$(ring))
195/181	192	192/167	177/171	τ_2(ring)
148	150	149	149	δ(CCC)
124	118	117	128	Intermolecular
111	106	105	112	intermolecular
88	96	96	93	τ_1(ring)
79	74	73	77	$\tau(C_5\text{-}C_{11})$
63	60	62	65	$\tau(C_{11}\text{-}C_{14})$

[a] See Table S1 for the definition of coordinates and Scheme 1 for atom numbering. Abreviations: s, symmetric; as, anti-symmetric; ν, stretching; δ, in-plane bending; γ, out-of-plane bending; τ, torsion, w, wagging; tw, twisting; n.obs., not observed; [b] Approximate description, with indication of only the proposed major coordinate contributing to the vibration (based on the calculated PEDs for the isolated molecule).

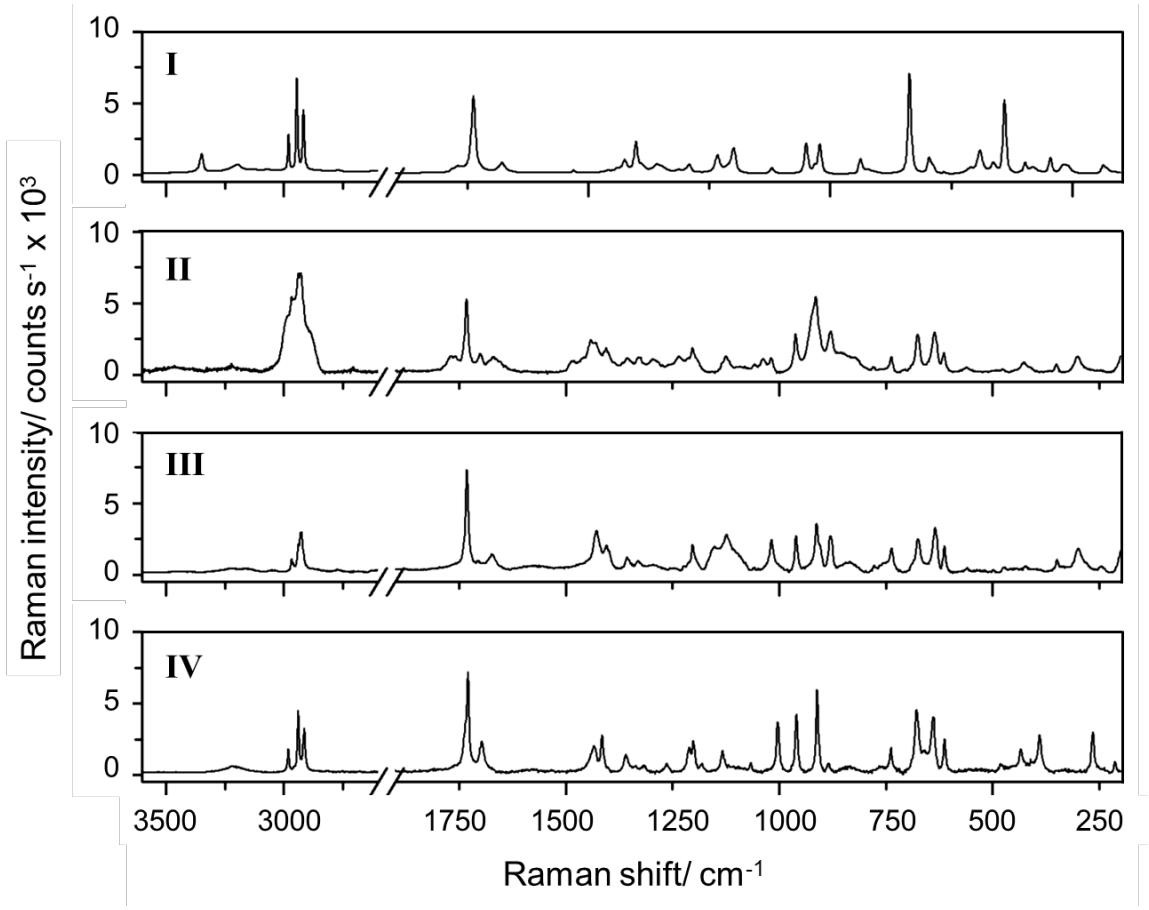

Figure 6. Raman spectra of polymorphs **I** to **IV** of 5AAH.

3.5 X-Ray diffraction (XRD) studies

A single-crystal X-ray diffraction study of polymorph **I** was undertaken at room temperature [293(2) K] on a good quality single-crystal, to compare with that reported at low-temperature [173 K].[36] Our measured X-ray data-set extended up to higher scattering angle and had better statistics (average $\frac{\sigma I}{I} = 0.0095$ and R_{eq} = 0.0237) than that in the low temperature study.

The molecule contains a chiral centre at C5, the absolute configuration of which could not be determined due to the absence of significant anomalous scattering at the Mo wavelength (Figure 7), despite the fact that an extensive set of Friedel pairs was measured with good statistics. The refinement was performed as a racemic twin without averaging the Friedel pairs (in contrast with the procedure used in the low temperature study that merged Friedel pais), but the refined value of the Flack parameter had, unsurprisingly, a too large error bar to establish the absolute configuration. Thus, similar to the situation encountered in,[36] we could not establish whether the

examined crystal resolved spontaneously from the solution as a crystal of a pure enantiomeric species or if it consists of a racemic twin.

Comparing the structure at room temperature to that determined at low temperature[36] we observe an excellent agreement between the two. As expected, and with the exception of those bonds involving H atoms, all others shrank in length by a small amount (<1%) upon cooling from room temperature down to 173 K. The variation of cell volume was -1.2% but, surprisingly, the *a* axis slightly expands on cooling whereas the *b* and *c* axis both contract, the largest variation occurring in the c axis. The results of the refined structure at room temperature have smaller error bars than those reported at low temperature, despite the larger thermal smearing, as result of better statistics and a larger number of reflections in our data set. The only remarkable difference found in the comparison of the refined structure at 293 K to that at 173 K is in the hydroxyl bond length, that extends from 0.80(3) Å to 1.02(4) Å, a feature that may represent a real displacement of the electron charge due to an increase of the hydrogen-bond interaction or arising from better localisation of the electron of the shared H atom at low temperature, due to a reduction of thermal motion.

The carboxylic planar side chain of the molecule (r.m.s. deviation for all non-H atoms = 0.0057 Å) is almost perpendicular [dihedral angle (173/293 K) = 89.28(6)º/88.6(6)º] to the planar hydantoin ring (r.m.s. = 0.024 Å for all non-H atoms). As was also observed in the low-temperature study, the hydroxy atom H17 points away from the hydantoin ring and the O–H bond and is *trans* to the C=O bond [O15=C14–O16–H17 dihedral equal to 180(2)º]. When compared with the results obtained for the isolated molecule, the conformation adopted by the 5AAH molecules in the crystal of polymorph **I** are remarkable. Indeed, in the crystal the molecules assume a conformation identical to that of the highest energy conformer for the isolated molecule, *i.e.*, *trans*-**III** (compare Figures 7 and 1). For the isolated molecule conformer *trans*-**III** the dihedral angle between the carboxylic planar side chain of the molecule and the hydantoin ring is 86.1º, which is identical to those found in the crystal of polymorph **I** at room or low temperature. The selection upon crystallization of a conformer that for the isolated molecule is not the absolute minimum energy structure is not a rare phenomenon, and it is on the basis, for example, of conformational polymorphism.[52] However, this is an extreme case that, to be best of our knowledge, has no parallel in the literature: conformational selection upon crystallization favours the highest-energy form among 13 different conformers of a molecule, which has an energy as large as ~40 kJ mol^{-1} higher than the conformational ground state (conformer *cis*-**I**). It is also clear that the change of conformation has to occur during crystallization, since in solution at room temperature this conformer shall have a negligible population

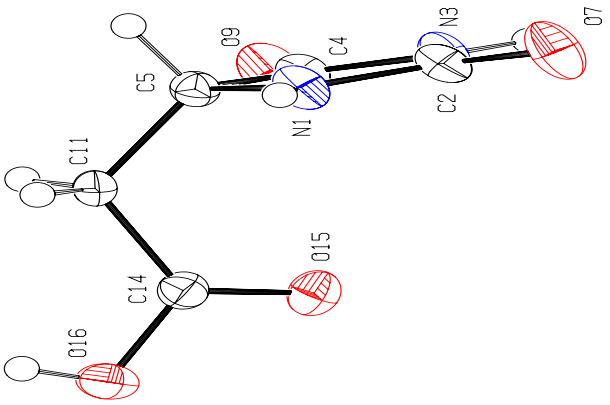

Figure 7. ORTEP plot of the molecule (polymorph I) showing the atom numbering scheme. Anisotropic displacement ellipsoids are drawn at the 50% probability level.

The hydrogen-bonding pattern in the crystal is similar to that reported in the low temperature study[36] and consists of (0 1 -2) planes of 5AAH molecules bound by O16–H17···O7, N1–H16···O16 and N3–H8···O9 hydrogen bonds. Further N1–H16···O16 and O16–H17···O7 hydrogen bonds interconnect these planes establishing a three-dimensional network. Interestingly, as remarked in[36] the N1 atom donates its H atom towards the carboxyl O16 atom rather than to the carbonyl one.

4. Conclusion

5-Acetic acid hydantoin was studied as an isolated molecule and in the neat solid phases. As isolated species, 5AAH was studied by matrix isolation infrared spectroscopy and DFT(B3LYP)/6-311++G(d,p) calculations. In the neat solid phases, the compound was investigated by DSC, PLTM, XRD and Raman spectroscopy.

The potential energy surface of the molecule was characterized thoroughly theoretically. Thirteen conformers were located, 6 of them having the carboxylic group in the *cis* arrangement (O=C–O–H dihedral equal to ~0º) and the other 7 in the *trans* configuration (O=C–O–H dihedral equal to ~180º). The relative energies and structures were obtained theoretically and discussed, also in comparison with those obtained for other molecules of the same family.[1-4] The electronic structure of the most stable conformer (*cis*-**I**) was analyzed using the NBO method, and used to rationalize details of the structure of the molecule. Particular emphasis was given to the

assessment of the specific characteristics of the σ and π electronic systems of the 5AAH molecule, and the stabilizing orbital interactions.

The IR spectrum of 5AAH monomeric form isolated in a low temperature argon matrix (*cis*-**I** conformer) was obtained and assigned. Assignments were supported by theoretical vibrational data, including normal coordinates' analysis.

The thermal study of the neat solid compound (by PLTM) allowed identification of five different polymorphs resulting from recrystallization in different solvents, which were also characterized by Raman spectroscopy. The crystal structure of the room temperature most stable polymorph (polymorph **I**), for which it was possible to obtain suitable crystals for single crystal structure determination, was refined, improving on previously reported data.[36]

On the whole, the performed investigations provided a comprehensive structural, spectroscopic and thermodynamic study of the targeted compound.

Supporting Information

Figure S1, with the DSC heating curve for polymorph I of 5AAH; Table S1, with the definition of the internal coordinates used in the normal modes' analysis; Table S2, with the B3LYP/6-311++G(d,p) optimized Cartesian coordinates of the different conformers of 5-acetic acid hydantoin. Tables S3 to S11 with the crystallographic data. The Supporting Information is available free of charge *via* the Internet at ...

Acknowledgements

The authors acknowledge financial support from the Portuguese Science Foundation ("*Fundação para a Ciência e a Tecnologia"* - FCT) – Projects CQC UIDB/00313/2020 and UIDP/00313/2020, also co-funded by FEDER/COMPETE 2020-EU. CFisUC is funded by FCT through the project UIDB/04564/2020 and UIDP/04564/2020. Access to instruments from Laser-Lab Coimbra and TAIL-UC facilities funded under QREN-Mais Centro is gratefully acknowledged. B.A.N. also acknowledges FCT for the SFRH/BD/129852/2017 PhD Scholarship.

References

(1) Ildiz, G. O.; Boz, I.; Unsalan, O. FTIR Spectroscopic and Quantum Chemical Studies on Hydantoin. *Opt. Spectrosc.* **2012**, *112*, 665-670.

(2) Ildiz, G. O.; Nunes, M. C.; Fausto, R. Matrix Isolation Infrared Spectra and Photochemistry of Hydantoin. *J. Phys. Chem. A* **2013**, *117*, 726-734.

(3) Nogueira, B. A., Ildiz, G. O., Canotilho, J.; Eusébio, M. E. S.; Fausto, R. Molecular Structure, Infrared Spectra, Photochemistry and Thermal Properties of 1-Methylhydantoin. *J. Phys. Chem. A* **2014**, 118, 5994-6008.

(4) Nogueira, B. A., Ildiz, G. O., Canotilho, J.; Eusébio, M. E. S.; Fausto, R. 5-Methylhydantoin: From Isolated Molecules in a Low-Temperature Argon Matrix to Solid State Polymorphs Characterization. *J. Phys. Chem. A* **2017**, *121*, 5267-5279.

(5) Wang, H.; Xiao, H.; Liu, N., Zhang, B. Shi, Q., Three New Compounds Dericed from Nitrofurantoin: X-Ray Structures and Hirshfeld Sueface Analyses. *Open J. Inorg. Chem.* **2015**, *5*, 63-73.

(6) Yu, F.-L.; Schwalbe, C. H.; Watkin, D. J.; Hydantoin and Hydrogen Bonding Patterns in Hydantoin Derrivatives. *Acta Crystallogr. Sect. C: Cryst. Struct. Commun.* **2004**, *60*, 714-717.

(7) U.K. Department of Health, *British Pharmacopoeia Online*; **2011**, Vols. I and II, monograph 1207.

(8) Finkel, M. J. Phenytoin Revisited. *Clin. Ther.* **1984**, *6*, 577–591.

(9) Zakrzewska, J. M.; McMillan, R. Trigeminal Neuralgia: The Diagnosis and Management of this Excruciating and Poorly Understood Facial Pain. *Postgrad. Med. J.* **2011**, *87*, 410–416.

(10) Konnert, L.; Reneaud, B.; de Figueiredo, R. M.; Campagne, J. M.; Martinez, J.; Colacino, E. Mechanochemical Preparation of Hydantoins from Amino Esters: Application to the Synthesis of the Antiepileptic Drug Phenytoin. *J. Org. Chem.* **2014**, *79*, 10132-10142.

(11) Fijisaki, F.; Shoji, K.; Shimodouzono, M.; Kashige, N.; Miake, F.; Sumoto, K. Antibacterial Activity of 5-Dialkylaminomethylhydantoins and Related Compounds. *Chem. Pharm. Bull. (Tokyo)* **2010**, *58*, 1123-1126.

(12) Kumar, C. S. A.; Kavitha, C. V.; Vinaya, K.; Prasad, S. B. B.; Thimmegowda, N. R.; Chandrappa, S.; Raghavan, S. C.; Rangappa, K. S. Synthesis and *in Vitro* Cytotoxic

Evaluation of Novel Diazaspiro Bicyclo Hydantoin Derivatives in Human Leukemia Cells: A SAR Study. *Invest New Drugs.* **2009**, *27*, 327-337.

(13) Kavitha, C. V.; Nambiar, M.; Kumar, C. S. A.; Choudhary, B.; Muniyappa, K.; Rangappa, K. S.; Raghavan, S. C. Novel Derivatives of Spirohydantoin Induce Growth Inhibition Followed by Apoptosis in Leukemia Cells. *Biochem. Pharmacol*. **2009**, *77*, 348-363.

(14) Yang, K.; Tang, Y.; Iczkowski, K. A. Phenyl-methylene Hydantoins Alter CD44-Specific Ligand Binding of Benign and Malignant Prostate Cells and Suppress CD44 Isoform Expression. *Am. J. Transl. Res*. **2010**, *2*, 88-94.

(15) Comber, R. N.; Reynolds, R. C.; Friedrich, J. D.; Manguikian, R. A.; Buckheit, R. W.; Truss, J. W.; Shannon, W. M.; Secrist, J. A. 5,5-Disubstituted Hydantoins: Syntheses and Anti-HIV Activity. *J. Med. Chem*. **1992**, *35*, 3567-3572.

(16) Marto, J.; Enisz, J.; Hosztafi, S.; Tímar, T. Preparation and Fungicidal Activity of 5-Substituted Hydantoins and Their 2-Thio Analogs. *J. Agric. Food Chem.* **1993**, *41*, 148-152.

(17) Nakajima, M.; Itoi, K.; Takamatsu, Y.; Kinoshita, T. Okazaki, T.; Kawakubo, K.,; Shindo, M.; Honma, T.; Tohjigamori, M.; Haneishi, T. Hydantocidin: a New Compound with Herbicidal Activity from *Streptomyces Hygroscopicus*. *J. Antibiot. (Tokyo)* **1991**, *44*, 293-300.

(18) Bhattacharjee, S.; Bhattacharya, S. Orotic Acid as Useful Supramolecular Synthon for the Fabrication of an OPV Based Hydrogel: Stoichiometry Dependent Injectable Behavior. *Chem. Commun.* **2015**, *51*, 6765-6768.

(19) Miura, M.; Masami, H.; Kakizawa, J.; Morita, A.; Uetani, T.; Yamada, K. Inhibitory Effect of L-Asparaginase in Lymphocyte Transformation Induced by Phyto-hemagglutinin. *Cancer Res.* **1970**, *30*, 768-772.

(20) Clemetson, C. A. B. Histamine Metabolism, in Vitamin C, Vol. III, Boca Raton, Fla; CRC Press; **1989**, 1-13.

(21) Clemetson, C. A. B., Is it a "Shaken Baby" or Barlow Disease Variant? *J. Am. Physic. Surg.*, **2004**, Vol. 9, 78-80.

(22) Chartterjee, I. B.; Majumder, A. K.; Nandi, B. K.; Subramanian, N. Synthesis of Some Major Functions of Vitamin C in Animals. *Ann. NY. Acad. Sci.* **1975**, *258*, 24-47.

(23) Sondhi, S.M.; Singh, J.; Kumar, A.; Jamal, H.; Gupta, P. P. Synthesis of Amidine and Amide Derivatives and Their Evaluation for Anti-Inflammatory and Analgesic Activities. *Eur. J. Med. Chem.* **2009**, *44*, 1010-1015.

(24) Taş, M.; Çamur, S.; Yolcu, Z.; Büyükgüngör, O. Synthesis, Crystal Structure, Spectroscopic and Thermal Properties of a Novel Complex of Hydantoin-5-acetic acid with Co(II). *J. Inorg. Organomet. Polym.* **2013**, *23*, 616-620.

(25) Bania, K.; Barooah, N.; Baruah, J. B. Structural Variations in Self-Assembled Cadmium Benzoate Complexes. *Polyhedron* **2007**, *26*, 2612-2620.

(26) Sabbah, R.; An, X. W.; Chickos, J. S.; Leitão, M. L. P.; Roux, M. V.; L. A. Torres, L. A. Reference Materials for Calorimetry and Differential Thermal Analysis. *Thermochim. Acta.* **1999**, *331*, 93-204.

(27) Bruker, APEX2, SAINT and SADABS, Bruker AXS Inc., Madison, Wisconsin, USA. 2014.

(28) Sheldrick, G. SHELXT - Integrated Space-Group and Crystal-Structure Determination, *Acta Crystallogr*. *A* **2015**, *71*, 3-8.

(29) Sheldrick, G. Crystal Structure Refinement with SHELXL, *Acta Crystallogr*. *C* **2015**, *71*, 3-8.

(30) Spek, A. Structure Validation in Chemical Crystallography. *Acta Crystallogr*. *D* **2009**, *65*, 148-155.

(31) Frisch, M. J.; Trucks, G. W.; Schlegel, H. B.; Scuseria, G. E.; Robb, M. A.; Cheeseman, J. R.; Scalmani, G.; Barone, V.; Mennucci, B.; Petersson, G. A. et al. Gaussian 09, Revision D.01, Gaussian, Inc. Wallingford CT. **2009**.

(32) Becke, A. D. Density-Functional Exchange-Energy Approximation with Correct Asymptotic Behavior. *Phys. Rev. A* **1988**, *38*, 3098-3100.

(33) Lee, C. T.; Yang, W.T.; Parr, R. G. Development of the Colle-Salvati Correlation Energy Formula into a Functional of Electron Density. *Phys. Rev. B* **1988**, *37*, 785-789.

(34) McLean, A. D.; Chandler, G. S. Contracted Gaussian-basis Sets for Molecular Calculations. 1. 2nd row atoms, Z=11-18. *J. Chem. Phys.* **1980**, *72*, 5639-5648.

(35) Lapinski, L.; Nowak, M. J. BALGA Suit of Computer Programs for PED Calculations, Institute of Physics, Polish Academy of Sciences, Warsaw.

(36) Gerhardt, V.; Tutughamiarso, N.; Bolte, M. Conformational Studies of Hydantoin-5-Acetic Acid and Orotic Acid. *Acta Cryst. C* **2012**, *68*, o92-o98.

(37) Fausto, R.; Batista de Carvalho, L. A. E.; Teixeira-Dias, J. J. C.; Ramos, M. N. *S-cis* and *S-trans* Conformers of Formic, Thioformic and Dithioformic Acids. An Ab Initio Study. *J. Chem. Soc. Faraday Trans. 2* **1989**, *85*, 1945-1962.

(38) Fausto, R. Bonding in Carbonyl and Thiocarbonyl Compounds: An Ab Initio Charge Density Study of H_2C=X and HC(=X)YH (X,Y= O or S). *J. Mol. Struct. Theochem.* **1994**, *315*, 123-136.

(39) Teixeira-Dias, J. J. C.; Fausto, R. A Molecular Mechanics Force Field for Conformational Analysis of Simple Acyl Chlorides, Carboxylic Acids and Esters. *J. Mol. Struct.* **1986**, *144*, 199-213.

(40) Maçôas, E. M. S.; Kriachtchev, L.; Pettersson, M.; Fausto, R.; Räsänen, M., Rotational Isomerism in Acetic Acid: The First Experimental Observation of the High-Energy Conformer. *J. Am. Chem. Soc.* **2003**, *125*, 16188.

(41) Kuş, N.; Fausto, R., Near-Infrared and Ultraviolet Induced Isomerization of Crotonic Acid in N_2 and Xe Cryomatrices: First Observation of Two High-Energy *Trans* C-O Conformers and Mechanistic Insights. *J. Chem. Phys.* **2014**, *141*, Art. Nº 234310.

(42) Maçôas, E. M. S.; Khriachtchev, L.; Pettersson, M.; Fausto, R.; Räsänen, M. Internal Rotation in Propionic Acid: Infrared Induced Isomerization in Solid Argon. *J. Phys. Chem. A* **2005**, *109*, 3617-3625.

(43) Teixeira-Dias, J. J. C.; Batista de Carvalho, L. A. E.; Fausto, R. The C_α-C Internal Rotation in α-Alkyl Substituted Carbonyls and Thiocarbonyls: $CH(CH_3)_2C$(=X)YH (X,Y= O or S). *J. Comput. Chem.* **1991**, *12*, 1047-1057.

(44) Fox, M. A.; Whitesell, J. K. Organische Chemie: Grundlagen, Mechanismen, Bioorganische Anwendungen. Springer, **1995**.

(45) Fausto, R.; Batista de Carvalho, L. A. E.; Teixeira-Dias, J. J. C.; Ramos, M. N. s-cis and s-trans Conformers of Formic, Thioformic and Dithioformic Acids. An Ab Initio Study. *J. Chem. Soc., Faraday Trans. 2* **1989**, *85,* 1945-1962.

(46) McKean, D. C. Individual CH Bond Strengths in Simple Organic Compounds: Effects of Conformation and Substitution. *Chem. Soc. Rev.* **1978**, *7*, 399-422.

(47) Castiglioni, C.; Gussoni, M.; Zerbi, G. Intramolecular Electrical and Dynamical Interactions in Formaldehyde: A Discussion Based on Infrared Intensity Data. *J. Chem. Phys.* **1985**, *82*, 3534-3541.

(48) Fausto, R. Bonding in Carbonyl and Thiocarbonyl Compounds: An Ab Initio Charge Density Study of $H_2C=X$ and HC(=X)YH (X,Y= O or S) *J. Mol. Struct. Theochem.* **1994**, *315*, 123-136.

(49) Wiberg, K. B.; Laidig, K. E. Rotational Barriers Adjacent to Carbonyl Groups 3. Amide Resonance and the C-O Barrier in Acids and Esters. *J. Am. Chem. Soc.* **1987**, *109*, 5935-5943.

(50) Rosado, M. T. S.; Jesus, A. J. L.; Reva, I. D.; Fausto, R.; Redinha, J. S. Conformational Cooling Dynamics in Matrix-isolated 1,3-Butanediol. *J. Phys. Chem. A* **2009**, *113*, 7499-7507.

(51) Reva, I. D.; Jesus, A. J. L.; Rosado, M. T. S.; Fausto, R.; Eusébio, M. E.; Redinha, J. S. Stepwise Conformational Cooling Towards a Single Isomeric State in the Four Internal Rotors System 1,2-Butanediol. *Phys. Chem. Chem. Phys.* **2006**, *8*, 5339-5349.

(52) Nogueira, B. A.; Castiglione, C.; Fausto, R. Color Polymorphism in Organic Crystals. *Comm. Chem.-Nature* **2020**, *3*, Art. Nº 34. https://doi.org/10.1038/s42004-020-0279-0

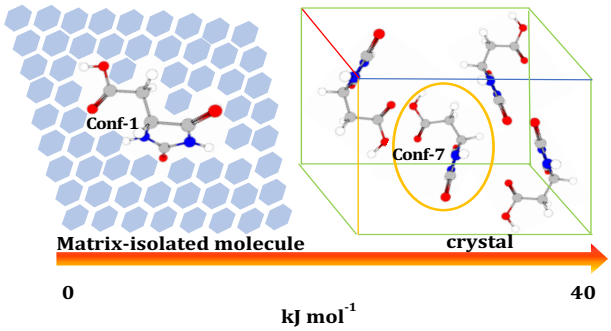

TOC Graphic

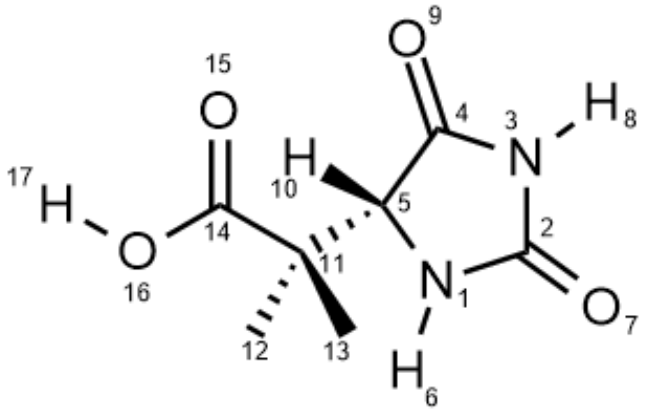

Scheme 1. The 5-acetic acid hydantoin molecule with the adopted atom numbering.

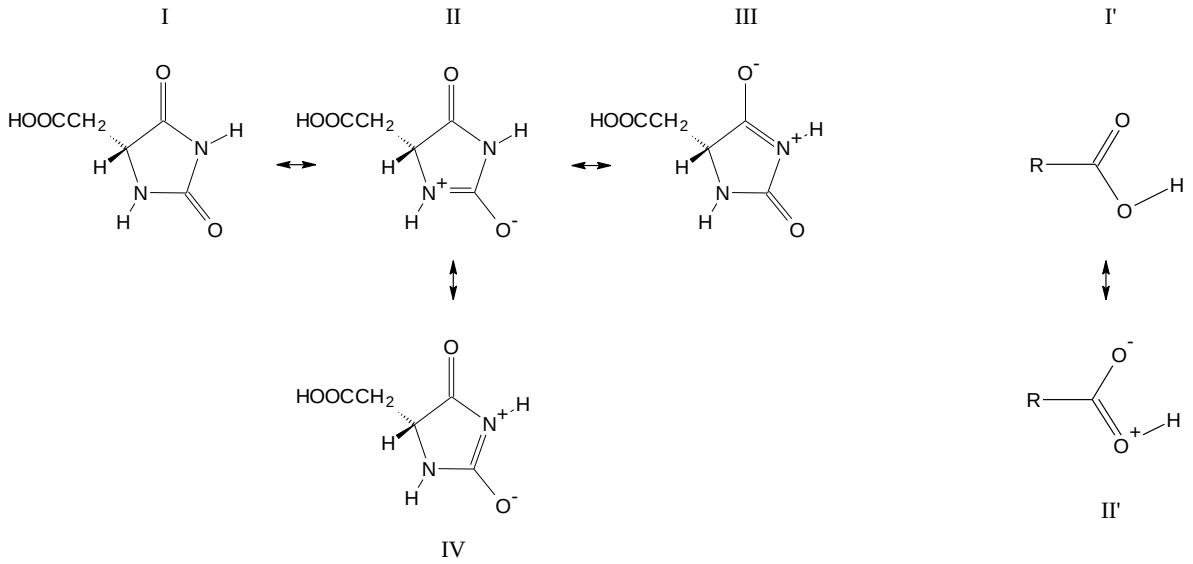

Scheme 2. I, I': Dominant canonic forms for 5AAH hydantoin ring and carboxylic acid fragment. II, III and IV: mesomeric structures assuming delocalization of π electrons in the NCO ring moieties of the molecule; II': mesomeric structure assuming delocalization of π electrons within the carboxylic acid fragment. R= hydantoin ring.

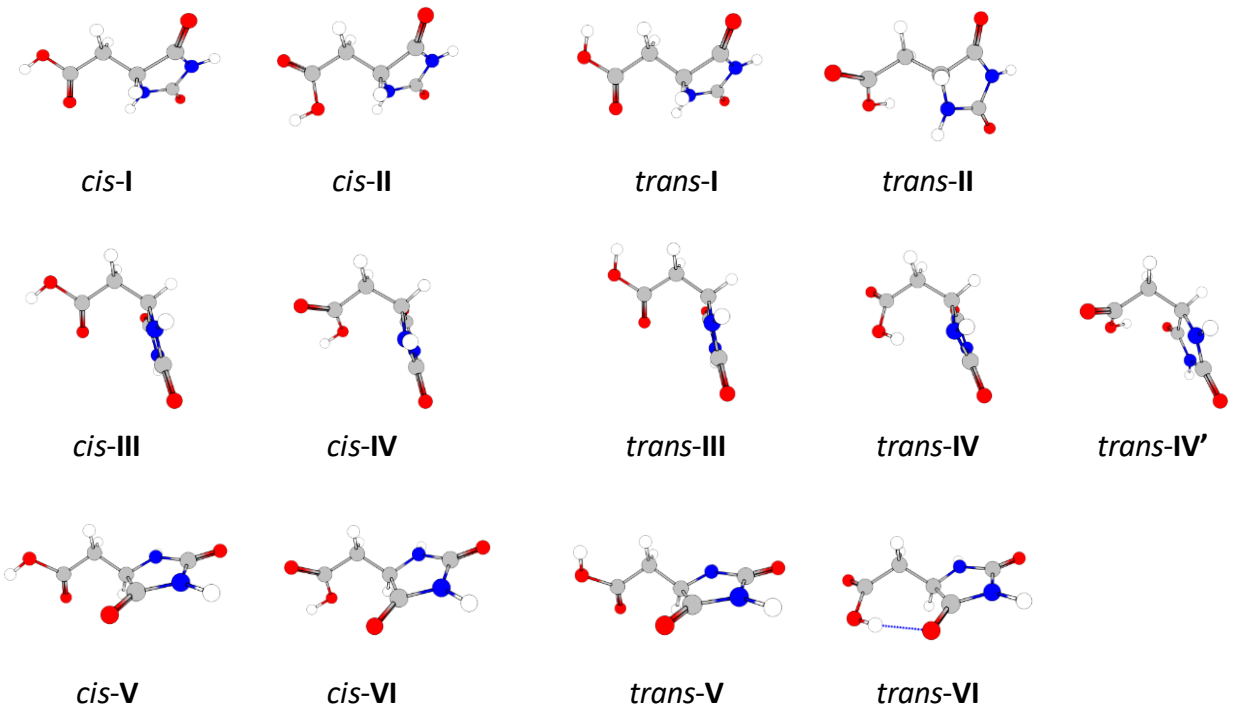

Figure 1. B3LYP/6-311++G(d,p) optimized geometries of the conformers of 5AAH (for energy data see Table II).

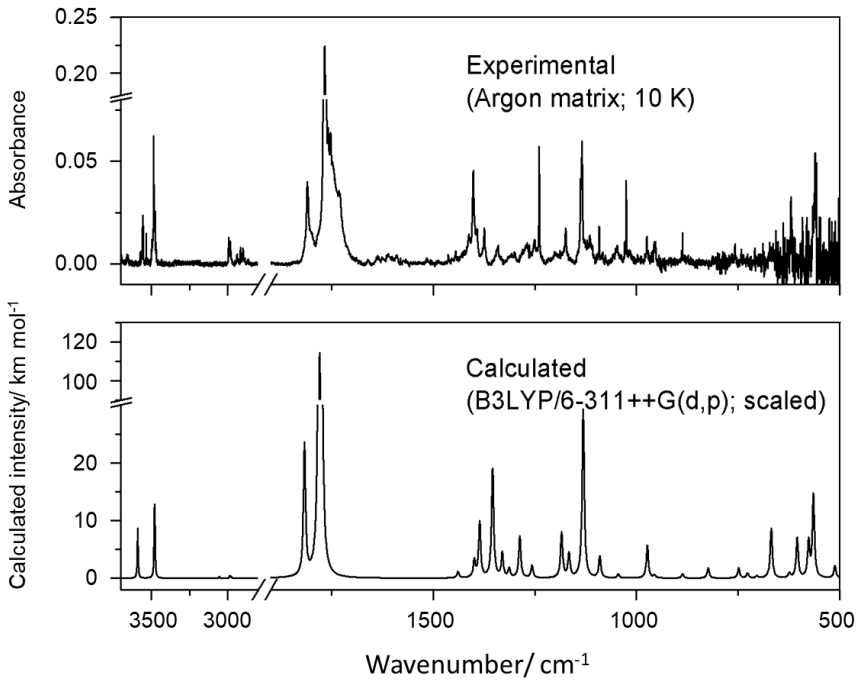

Figure 2. Experimental infrared spectrum of monomeric 5AAH isolated in an argon matrix at 10 K (*top*) and simulated spectrum of conformer *cis*-I, using Lorentzian functions centered at the scaled B3LYP/6-311++G(d,p) calculated wavenumbers, with calculated intensities corresponding to areas below the bands (*bottom*).

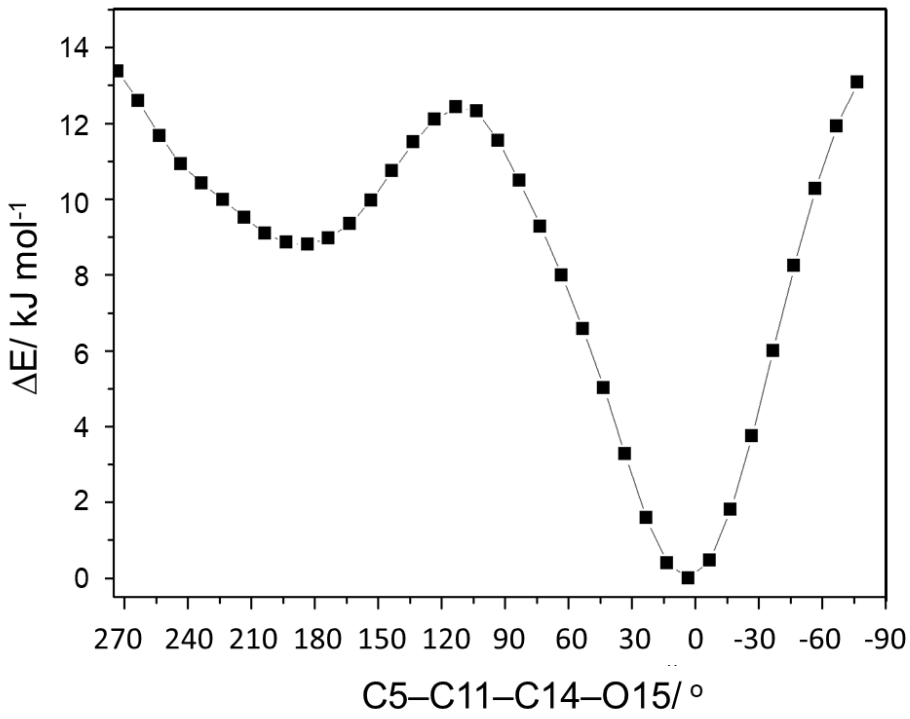

Figure 3. B3LYP/6-311++G(d,p) calculated potential energy profile for interconversion between conformers *cis*-**I** and *cis*-**II**.

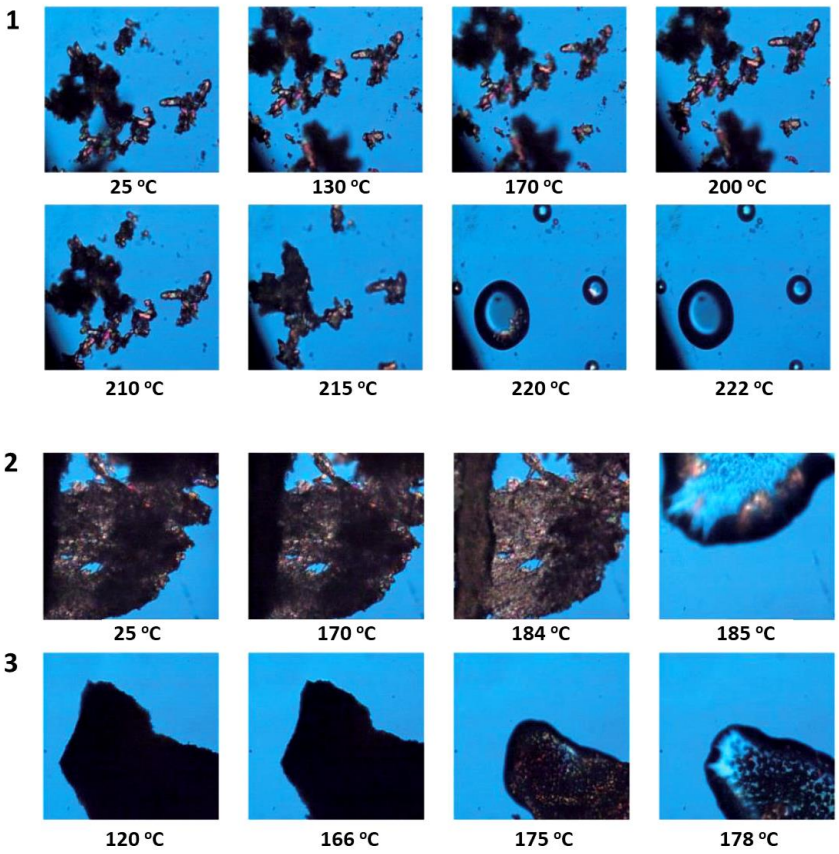

Figure 4. Polarized light thermal microscopy images collected during heating of polymorphs **I** (part 1; *top*), **II** (part 2; *middle*) and **III** (part 3; *bottom*) of 5AAH from 25 ºC to about their melting temperatures (heating rate: 10 ºC min^{-1}, amplification 200x).

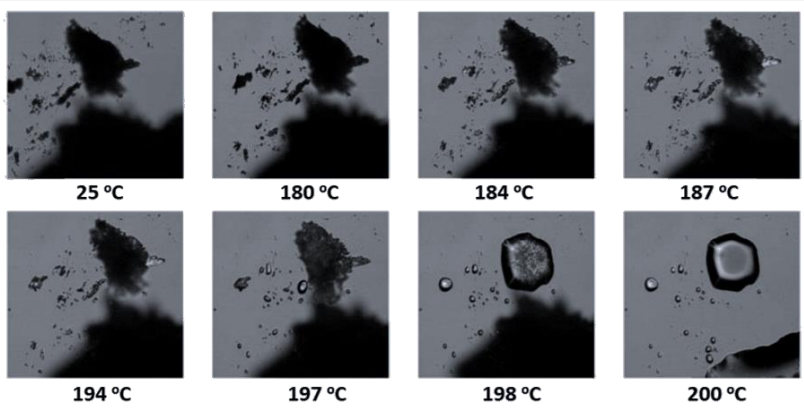

Figure 5. Polarized light thermal microscopy images collected during heating of an initial sample of polymorph **IV** of 5AAH from 25 to 200 ºC (heating rate: 10 ºC min^{-1}, amplification 200x). The **IV→V** solid-solid transition is observed at *ca.* 180-185 ºC, with the melting of the generated polymorph **V** being observed at *ca.* 198-200 ºC.

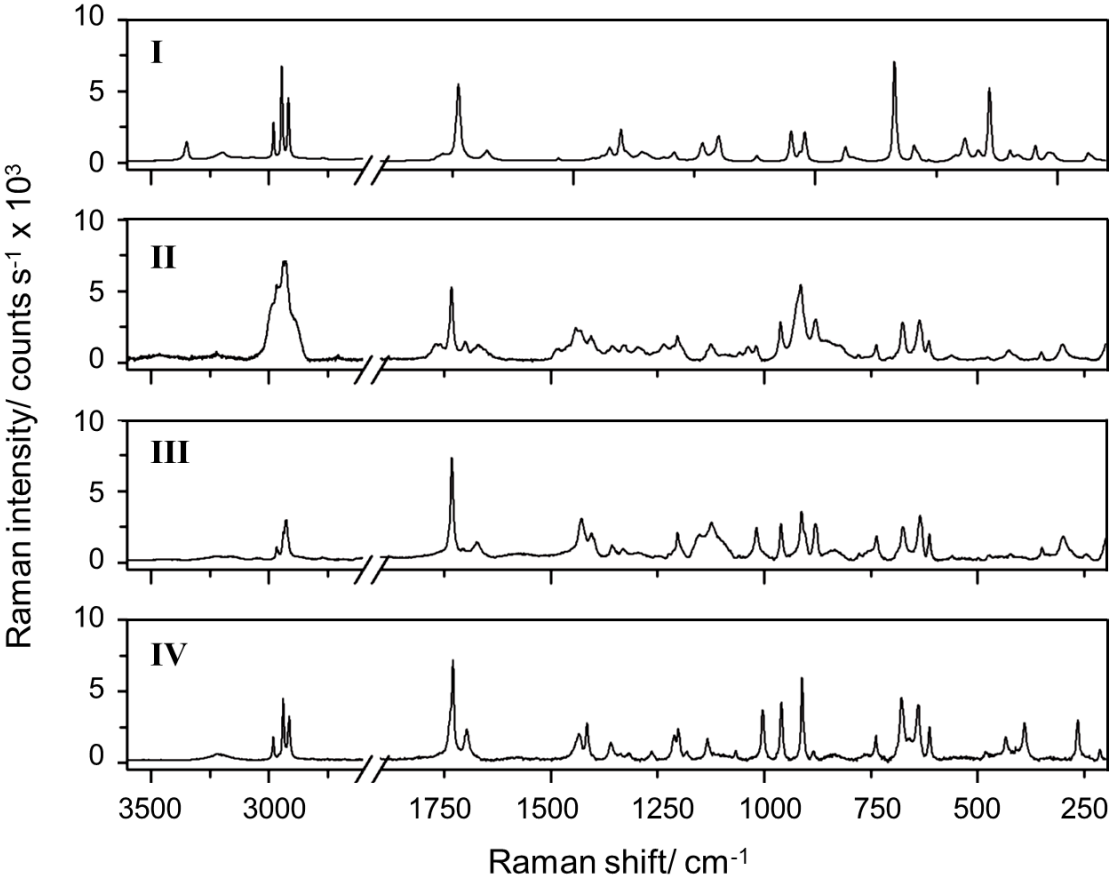

Figure 6. Raman spectra of polymorphs **I** to **IV** of 5AAH.

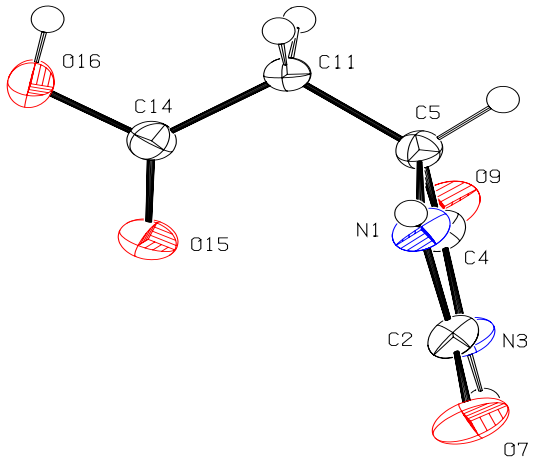

Figure 7. ORTEP plot of the molecule (polymorph I) showing the atom numbering scheme. Anisotropic displacement ellipsoids are drawn at the 50% probability level.